Syntaxin11 Deficiency Inhibits CRAC Channel Priming to Suppress Cytotoxicity and Gene Expression in T Lymphocytes.

Sritama Datta[1#], Abhikarsh Gupta[1#], Kunal Mukesh Jagetiya[1], Resmi Bera[1], Vikas Tiwari[2⊥], Atharva Rahul Yande[1], Megumi Yamashita[3⊥], Abdul Rishad, Vishal Malik[1], Sreejith Raran-Kurussi[1], Sandra Ammann[4,5], Mohammad Shahrooei[6], Kalyaneswar Mandal[1], Ramanathan Sowdhamini[2], Murali Prakriya[3], Adish Dani[1], Monika Vig[1]*

Address and Affiliation: [1]Tata Institute of Fundamental Research, Hyderabad, India. [2]National Centre for Biological Sciences, Bangalore, India. [3]Northwestern University, Feinberg School of Medicine, Chicago, USA. [4]Institute for Immunodeficiency, University of Freiburg, Germany. [5]Institute for Transfusion Medicine and Gene Therapy, University of Freiburg, Germany. [6]Department of Microbiology, Immunology and Transplantation, Clinical and Diagnostic Immunology, KU Leuven, Leuven, Belgium.

[#, ⊥] These authors contributed equally.

***Correspondence to:** monika.vig@gmail.com

Keywords: Orai, FHLH4, CRAC, Syntaxin11, SOCE, calcium, Stim, SNARE, ion channels, immunodeficiency, cytotoxicity, CTL, CD8 T lymphocytes

Abstract:

Mutations in Syntaxin11, a Q-SNARE, result in a fatal immune disorder known as familial hemophagocytic lymphohistiocytosis 4 (FHLH4) in human patients. A key diagnostic feature of FHLH4 is defective T and natural killer (NK) cell cytotoxicity. Here we show that Syntaxin11 directly binds and regulates Orai1, the pore forming subunit of calcium release activated calcium (CRAC) channels. CRAC channels enable store-operated calcium entry (SOCE) from the extracellular space and are crucial for granule exocytosis and nuclear factor of activated T cells (NFAT) dependent gene expression in activated lymphocytes. Syntaxin11 depletion strongly inhibited SOCE, CRAC currents, NFAT activation, interleukin-2 gene expression and degranulation in FHLH4 patient T lymphocytes and cell lines. Remarkably, defects of granule exocytosis as well as interleukin-2 expression could be reversed by ionomycin in patient T lymphocytes and a constitutively active, H134S, mutant of Orai1 rescued calcium entry in Syntaxin11 depleted cells. Further analyses showed that Syntaxin11 primes Orai1 for optimal on-site multimeric assembly which was Stim independent but required for gating. Priming of ion channel pore subunits is, therefore, a primary function of specific SNAREs which may have preceded their role in vesicle fusion.

63 **Introduction:**

64

65 Familial hemophagocytic lymphohistiocytosis 4 (FHLH4) is a life-threatening
66 immune disease caused due to mutations of STX11 [1]. The underlying cause of FHLH
67 is reduced cytolytic activity of T and NK cells [2], which renders patients susceptible to
68 recurrent infections. Patients suffer from high fever, severe lymphopenia in early infancy
69 and succumb to disease by adolescence, unless given bone marrow transplants. STX11
70 is highly expressed in almost all cells of the immune system and, being a Q-SNARE, is,
71 by default, associated with exocytosis of vesicles. Intriguingly, FHLH4 patients also
72 manifest cytokine storm, which cannot be reconciled with a presumed general defect in
73 membrane trafficking and vesicle fusion.

74

75 Most eukaryotic cells have a limited amount of calcium sequestered inside
76 intracellular stores, the largest of which is the endoplasmic reticulum (ER). Signaling from
77 cell surface receptors induces the release of stored calcium which, in turn, activates store-
78 operated calcium entry (SOCE) to replenish stores, sustain signaling and drive other
79 calcium dependent cellular processes [3]. Calcium release activated calcium (CRAC)
80 channels are the major conductors of SOCE [4]. In lymphocytes and mast cells, CRAC
81 currents have been shown to be crucial for cytotoxicity, degranulation as well as gene
82 expression [5, 6]. Working in concert with a number of accessory proteins, Orai (CRACM)
83 multimers conduct SOCE upon functional clustering with Stim proteins in ER-PM
84 junctions [7-9]. Yet, the prevailing thought attributes all structural transitions that result in
85 the activation of CRAC currents to Stim proteins [10].

86

87 Genome-wide RNAi screens, which initially identified Orai (CRACM), have also
88 yielded a wealth of information regarding additional crucial players in SOCE [8, 11, 12].
89 For instance, we have previously shown that alpha-soluble N-ethylmaleimide sensitive
90 factor (NSF) attachment protein (α-SNAP), a well-known synaptic family adaptor protein
91 that forms a part of the 20S SNARE super-complex [13], is a crucial component of the
92 CRAC channel supramolecular complex [8, 9]. α-SNAP independently binds Stim as well
93 as Orai and is required for the correct assembly and calcium selectivity of CRAC channels

[14-16]. α-SNAP depletion in cells revealed that Stim:Orai coupling is necessary but not sufficient for SOCE, a process that requires distinct time-resolved molecular steps *in vivo*.

In addition to α-SNAP, SNAREs also came up as candidates in two genome wide RNAi screens for regulators of SOCE but were not characterized [8, 12]. Furthermore, specific SNAREs have been previously found to form inhibitory associations with specific ion channels, but their exact role was not defined [17]. Therefore, we hypothesized a more fundamental function for the association of SNAREs with ion channel pore subunits and set out to test this in the context of SOCE. Using a targeted RNAi screen, biochemical and biophysical analyses, we have found a direct role of STX11 in facilitating assembly of CRAC channel pore subunit, Orai1, into optimal multimers. Assembly of Orai1 was independent of, and preceded, trapping and gating by Stim1. Analyses of T cells derived from symptomatic STX11 deficient, FHLH4 patient showed that the previously reported [2], as well as newly identified, defects in degranulation and interleukin-2 gene expression predominantly stem from suppressed SOCE. Based on the findings presented here, we demonstrate a novel SNARE dependent priming step for CRAC channel pore in the molecular sequence of SOCE and suggest preventive pharmacological interventions for FHLH4 patients.

125 **Results:**

126 RNAi dependent ablation of a Q-SNARE, Syntaxin 5 (STX5), has earlier shown
127 inhibition of SOCE in a genome-wide screen performed in *Drosophila* S2 cells [12] and
128 STX1A has been previously shown to bind a variety of ion channels [17]. Therefore, we
129 first knocked down STX5 (Supplementary Figure 1A) and STX1A (Supplementary Figure
130 1B) using different sequences of shRNA targeting each gene in HEK293 cells and
131 measured SOCE in response to Thapsigargin (TG). In both cases, we did not see a
132 significant defect in SOCE. Since several proteins involved in synaptic function are not
133 ubiquitously expressed and many show redundancy in function, we searched online
134 databases to target SNAREs that are expressed in HEK293 and/or T cells
135 (Supplementary Figure 1C-H). We found that Syntaxin11 knockdown showed strong and
136 consistent inhibition of SOCE by day 3 to 4 (Supplementary Figure 2A-B) (Figure 1A-B).
137 Quantitative PCR (qPCR) analysis of total RNA extracted from scramble (scr) and STX11
138 shRNA treated cells showed nearly 70% depletion of STX11 mRNA (Supplementary
139 Figure 2C) and ectopic expression of STX11 in STX11 depleted Jurkat cells rescued
140 SOCE (Figure 1C,D). The efficiency of STX11 depletion was assessed for each
141 experiment reported in this study. We restricted our analysis to day 3 to 4, post RNAi
142 treatment, as longer incubations with RNAi or CRISPR knockout of STX11 affected cell
143 viability.

144

145 Given that STX11 is highly expressed in most immune cells and is the only known
146 SNARE that, when mutated, causes defects in T and NK cell cytotoxicity in humans and
147 mice [2], we hypothesized that reduced SOCE contributes to the cytotoxicity defects of
148 FHLH4 patient T cells. To test this hypothesis, we isolated PBMCs from an FHLH4 patient
149 with a homozygous deletion frameshift mutation in the STX11 coding sequence,
150 c.752delA:p.Lys251fs. The patient presented with all symptoms of FHLH4 disease by 4
151 years of age. Given the limited sample amount, we expanded PBMC numbers by
152 periodically stimulating patient and healthy donor cells with PHA and IL-2, prior to
153 analysis. Isolation and Sanger sequencing of DNA from patient PBMCs showed deletion
154 of a single Adenine at position 752 in the STX11 gene which lead to frameshift following
155 Lysine 251 (Figure 1E). The absence of any contaminating wildtype peaks showed that

156 the mutation was present in all blood cells. Figure 1F shows schematic of the predicted
157 mutant STX11 protein with an estimated molecular weight of ~39.5 KDa compared to ~33
158 KDa of wildtype STX11. The frameshift mutation resulted in disruption of the SNARE
159 domain, ablation of the terminal cysteines and elongation of the resulting transcript. We
160 subjected whole cell lysates prepared from the FHLH4 patient and healthy donor (HD)
161 PBMCs to SDS-PAGE and western blot and found that while the wildtype STX11 band
162 was absent, a faint but distinct band running at ~37 KDa was present in the FHLH4 patient
163 sample lysate (Figure 1G). Therefore, the predicted and observed molecular weight of
164 the FHLH4 mutant protein was higher but its levels appeared significantly reduced
165 compared to STX11 from HD. This is likely due to protein instability and degradation
166 because ectopic expression of the FHLH4 STX11 mutant in HEK293 cells showed at least
167 two clear bands (Figure 1H), although reduced reactivity to anti-STX11 antibody is also a
168 possibility. In accordance with our findings in the STX11 depleted cell lines (Figure 1A-B
169 and Supplementary Figure 2A-B), SOCE was found to be significantly defective in FHLH4
170 T cells when compared to HD (Figure 1I). Further, expression of wildtype (Figure 1J), but
171 not FHLH4 mutant STX11 (Figure 1K-L), reversed defective SOCE in STX11 deficient
172 patient (Figure 1J) and Jurkat T cells (Figure 1K-L), respectively. These data suggest that
173 FHLH4 mutant STX11 was functionally compromised in addition to being unstable and
174 no additional unknown mutations resulted in reduced SOCE.
175
176 To determine whether the inhibition of SOCE in Figure 1 resulted from changes in
177 the activity of CRAC channels or their expression level, we quantified the level of Orai1
178 expression in plasma membrane. To do this, we labelled a previously characterized
179 U2OS cell line stably expressing Orai1 tagged with a bungarotoxin binding site (BBS) in
180 the extracellular loop and YFP in the C-terminus (Orai-BBS-YFP) with Alexa-647
181 conjugated alpha-bungarotoxin (BTX-A647) (Supplementary Figures 3A) [9]. There was
182 no change in the expression of total Orai1 in the PM of STX11 depleted U2OS cells
183 (Supplementary Figure 3B), even though SOCE was significantly suppressed
184 (Supplementary Figures 3C-D). The ER-targeted CEPIA expressing control and STX11
185 depleted cells showed comparable ER calcium content (Supplementary Figure 3E).
186 Labelling STX11 depleted cells with ER, Golgi organelle specific markers also showed no

187 abnormalities (Supplementary Figures 3F-G) suggesting that the overall health, function
188 and calcium content of Golgi and ER were not adversely affected by STX11 depletion.
189
190 Previous studies have shown that SOCE in T cells is mediated by CRAC channels
191 formed by Orai proteins. To test whether CRAC current (I_{CRAC}) was affected by
192 knockdown of STX11 in T cells, we performed whole cell patch clamp recordings on
193 scramble and STX11 shRNA treated Jurkat T cells (Figure 2A-B). Leak-subtracted I_{CRAC}
194 was recorded in 20 mM Ca^{2+} and a Na^{+}-based divalent cation free (DVF) solution. These
195 recordings showed that both the Ca^{2+} and DVF CRAC currents were significantly
196 decreased in the STX11 shRNA treated cells with the normalized currents shown in
197 Figure 2C. The electrophysiological properties of the residual current in STX11 shRNA
198 treated cells was indistinguishable from I_{CRAC} in scramble shRNA treated cells in terms of
199 blockade of the Ca^{2+} current by La^{3+} and depotentiation of the DVF current over tens of
200 seconds. Moreover, the reversal potential of the Ca^{2+} and DVF currents were similar
201 between scramble and STX11 shRNA treated Jurkat T cells, suggesting that STX11
202 depletion does not affect the calcium selectivity of CRAC channels (Figure 2D). Together,
203 these results demonstrate that STX11 works by specifically modulating I_{CRAC} in T cells.
204
205 CRAC channel mediated sustained calcium influx is crucial for the activation of a
206 key calcium dependent transcription factor known as nuclear factor of activated T cells
207 (NFAT) [4, 18]. We stimulated control and STX11 depleted Jurkat T cells with
208 Thapsigargin (TG)+PMA, prepared nuclear, cytosolic extracts and subjected them to
209 western blot using anti-NFAT1 antibody (Figure 3A). Nuclear translocation of NFAT was
210 severely compromised in STX11 depleted T cells. In addition, immunofluorescence
211 imaging and quantification of total *versus* nuclear NFAT from anti-CD3 stimulated Jurkat
212 cells showed a defect in nuclear translocation of NFAT1 in STX11 depleted cells (Figure
213 3B-C). To determine whether NFAT induced gene expression was affected [4, 18], we
214 quantified IL-2 mRNA by qPCR and secreted IL-2 levels from culture supernatants of anti-
215 CD3 stimulated Jurkat T cells. STX11 depleted cells showed a significant decrease in IL-
216 2 gene expression as well as secretion (Figure 3D, 3E). We stimulated HD and FHLH4
217 patient T cells either through T cell receptor using anti-CD3 or with phorbol myristate

218 acetate (PMA) + Ionomycin and assessed IL-2 gene expression. Importantly, induction of
219 IL-2 expression was significantly defective in FHLH4 patient T cells but could be largely
220 restored with Ionomycin (Figure 3F). We next performed granule release assay on the *in*
221 *vitro* cultured HD and FHLH4 patient CD8 T cells in response to anti-CD3 mediated
222 stimulation and observed a significant defect in the FHLH4 patient CD8 T cell
223 degranulation (Figure 3G, 3H). To determine whether the reduced granule release results
224 from a direct defect in vesicle fusion or SOCE, we stimulated cells with Ionomycin along
225 with (PMA). Remarkably, CD8 T cell degranulation was fully restored in FHLH4 T cells
226 suggesting that defective SOCE primarily causes cytolytic defects in FHLH4 T cells. Of
227 note, the patient exhibited all symptoms of FHLH4 disease and we observed strong
228 suppression of SOCE (Figure 1I), IL-2 gene expression and secretion (Figure 3D-F).
229 However, *in vitro* culture of FHLH4 patient CD8 T cells with IL-2 has been previously
230 shown to partially or fully restore cytolytic defects by other groups [19, 20]. Therefore,
231 considering previous reports, a relatively lower (50%) defect in CD8 T cells degranulation
232 was not surprising [19, 20]. Collectively, these data suggest that defects in T cell
233 degranulation as well as interleukin-2 gene expression originate from suppressed SOCE
234 and significantly contribute to the immune dysregulation of FHLH4 patients.
235
236 Unlike most Q-SNAREs, STX11 lacks a transmembrane domain but harbors a
237 stretch of cysteines proposed to be essential for its membrane localization close to the C-
238 terminus (Supplementary Figure 4A) [21]. The cellular localization of STX11 is not
239 established because, unlike primary T cells, native STX11 is undetectable in Jurkat and
240 HEK293 cell lines using available commercial antibodies. Tagging STX11 on either N- or
241 C-terminus results in partial degradation (Supplementary Figure 4B) and complete mis-
242 localization of the protein (Supplementary Figure 4C). Therefore, we inserted an HA tag
243 inside the N-terminal unstructured region of human STX11. The internal HA tagged
244 STX11 as well as un-tagged STX11 localized in the plasma membrane of most HEK 293
245 cells (Figure 4A) and co-localized with Orai1-YFP in cells co-expressing Orai1 (Figure
246 4B). To test whether STX11 and Orai1 formed a complex, we co-expressed STX11 with
247 either Flag- or Myc-tagged Orai1 in HEK293, prepared whole cell lysates (WCLs) and
248 subjected them to co-immunoprecipitation (co-IP) followed by western blot using either

249 anti-Flag, anti-Myc or anti-STX11 antibodies. Both Orai1 and STX11 could co-IP each
250 other (Figure 4C-D). To further assess whether STX11 directly bound Orai1, we
251 expressed and purified from *E. coli*, MBP-tagged N- and C-terminal cytosolic tails of Orai1
252 (Figure 4E). *In vitro* pull-down assay performed by incubating MBP-tagged Orai1
253 cytoplasmic tails with full length soluble His-tagged STX11 showed that the C-terminus
254 of Orai1 directly bound STX11 (Figure 4F). SNAREs typically utilize their SNARE domain
255 for associating with other SNAREs [22]. To identify the domain of STX11 involved in the
256 regulation of SOCE, we expressed His-tagged H_{abc} and SNARE domains of STX11 in *E.*
257 *coli*, purified and assessed their binding to the MBP-tagged Orai1 tails using pull-down
258 assay. We found that the H_{abc} domain of STX11 bound to the C-terminus of Orai1 (Figure
259 4G). The SNARE domain of STX11 did not show any binding to Orai1 and only a faint
260 binding to SNAP23 (Supplementary Figure 4D). We next used AlphaFold3 (AF3) to obtain
261 deeper insights into the domain interactions of STX11 and Orai1. Of all the possible
262 combinations, the complex of STX11 H_{abc} and Orai1 C-terminus resulted in a significantly
263 high prediction score (Supplementary Table 1). We, therefore, executed AF3 predictions
264 with different initial seeds to generate multiple models of STX11 H_{abc} with Orai1 C-
265 terminus. We calculated the contact frequency of interface residues in different models
266 and found that multiple residues showed frequency greater than 0.8 (Supplementary
267 Figure 5A). For further analysis, we considered the predicted model with the best score
268 (Supplementary Table 2). Next, we performed all-atom MD simulation in aqueous
269 environment (Movies 1-3) to assess the conformation, interaction stability of the STX11
270 H_{abc} and Orai1 C-terminus complex, which was stable throughout the simulation time
271 suggested by RMSD (Supplementary Figure 5B), and binding free energy (ΔG) values
272 (Supplementary Figure 6A) (Figure 4H). The individual trajectories were concatenated
273 and clustered to obtain a centroid structure for this complex. There were 46 clusters, and
274 the largest cluster, with 52 members, showed an elaborate protein-protein interface where
275 STX11 H_{abc} was found to be oriented in an anti-parallel orientation to the Orai1 C-terminus
276 (Figure 4I).
277 Because STX11 binds the C-terminus of Orai1 and the region largely overlaps with
278 the Stim1 binding domain, we next sought to determine whether STX11 clusters with
279 Orai:Stim puncta. We over-expressed HA-tagged STX11 in a Orai1-YFP and CFP-Stim1

expressing stable HEK293 cell line, store-depleted with TG, and stained using anti-HA antibody. We did not observe co-clustering of STX11 in Orai:Stim puncta even 8 minutes post store-depletion (Figure 4J-K). Accordingly, STX11 did not co-IP with Stim1 in store-depleted cells (Supplementary Figure 7A). These data suggest that STX11 comes off Orai1 C-terminus prior to Stim1 dependent clustering of Orai1. Since co-IP studies suggested sustained interaction between STX11 with Orai1 (Figure 4B-C), we quantified the fraction of Orai1 that resides inside Stim:Orai puncta w.r.t total Orai1 in PM and found that post TG addition, nearly 60% of Orai1 remains outside of Stim1 puncta even in unmanipulated cells (Supplementary Figure 7B). We used AF3 to generate the complex of Stim-Orai activating region (SOAR) domain of Stim1 and Orai1 (Supplementary Figure 8A). Given that SOAR is a dimer under resting state, we used two copies each of SOAR and Orai1 [23] [24]. The prediction scores for their complex are shown in Supplementary Table 3. The best scoring model among multiple runs of AF3 was considered for MD simulations on the complex of Orai1 C-terminus (256-301) and SOAR. The ΔG values for the complex are shown in (Supplementary Figure 8B-C). Three independent MD simulations were run for the complex (Movies 4-6) which showed an initial conformational change which stabilized thereafter (Supplementary Figure 9A). All three simulation trajectories were concatenated and clustered to obtain a centroid structure for this complex (Supplementary Figure 9B). There were 43 clusters, and the largest cluster had 77 structures. Collectively, these data suggest that STX11 directly binds Orai1 with an affinity that is physiological but relatively poorer when compared to the binding of SOAR dimers to Orai1. Therefore, presence of high density of SOAR dimers in ER-PM junctions of store-depleted cells could potentially outcompete STX11:Orai1 interactions by progressively allowing formation of SOAR:Orai1 oligomers. It is also possible that another, yet to be characterized, molecular step and/or protein actively catalyzes the removal of STX11 from Orai1 prior to its entrapment in ER-PM puncta. Future studies will be able to systematically assess these possibilities.

The major interactions predicted between STX11 and Orai1 from all-atom MD simulations are highlighted in Supplementary Figure 6B-C. To assess the significance of these interactions, we performed site-directed mutagenesis of two key residues of STX11 predicted to be involved in binding to Orai1 (Figure 5A). Ectopic expression of untagged

311 N147A_E150A STX11 showed correct localization (Figure 5A) as well as stable
312 expression (Figure 5B) but failed to rescue SOCE in STX11 depleted Jurkat T cells
313 (Figure 5C-D). We next expressed His-tagged wildtype and N147A_E150A mutant
314 STX11 in *E. coli.*, purified (Figure 5E) and assessed their ability to bind MBP-tagged Orai1
315 C-terminal tail in an *in vitro* pull-down assay (Figure 5F). Compared to wildtype STX11,
316 N147A_E150A mutant STX11 showed reduced binding to Orai1 C-terminus. Further, we
317 introduced four mutations, R289A_E272A_E275A_E278A, in the Orai1 C-terminus
318 (Figure 5G), tagged with YFP and expressed in HEK293 cells. The Orai1 mutant localized
319 to PM (Figure 5G) but failed to rescue SOCE in Orai1 deficient cells (Figure 5H-I). We
320 expressed and purified MBP-tagged R289A_E272A_E275A_E278A mutant Orai1 C-
321 terminus from *E. coli* and assessed its ability to bind purified wildtype as well as
322 N147A_E150A mutant STX11 in a pull-down assay (Figure 5J). Binding of Orai1 mutant
323 to both was significantly compromised. Because Stim1 binds an overlapping region of the
324 Orai1 C-terminus, we next tested whether mutation of Orai1 residues affected Stim1
325 binding. We co-expressed YFP-tagged soluble CRAC activation domain (CAD) of Stim1
326 (YFP-CAD) (Figure 5K) with either CFP-tagged wildtype or mutant Orai1 in HEK293 cell
327 line. YFP-CAD localizes to the cytosol in HEK293 cells but in cells overexpressing Orai1,
328 a significant fraction of it localizes to plasma membrane due to its association with Orai1
329 [10]. We quantified relative YFP-CAD levels in the plasma membrane of both groups
330 (Figure 5K-L) but found no difference in the PM recruitment of CAD suggesting that the
331 inability of R289A_E272A_E275A_E278A mutant Orai1 to support SOCE does not result
332 from defective binding to CAD/SOAR. Collectively, these data demonstrate a direct role
333 of STX11 in the binding and regulation of Orai1.

334 Upon store depletion, Stim1 localizes to ER-PM junctional regions where it traps
335 and co-clusters with Orai1. To further understand the mechanism, we first imaged
336 HEK293 cells expressing CFP-Orai1, Stim1-YFP under resting conditions and then
337 quantified the levels of Orai1 and Stim1 in ER-PM junctions (puncta) of store-depleted
338 control and STX11 depleted cells. The distribution of Orai1 and Stim1 was normal in
339 resting cells (Figure 6A). However, in store-depleted cells, clustering of CFP-Orai1 was
340 visibly defective in STX11 RNAi treated cells (Figure 6B), even though the intensities
341 (Figure 6C) and area of Stim1-YFP puncta were normal (Figure 6D). Quantification of

342 Orai1 intensities confirmed a defect in entrapment (Figure 6E) with relatively higher
343 fraction of Orai1 present outside Stim1 puncta in STX11 depleted cells (Figure 6F). To
344 determine whether reduced clustering of Orai1 resulted from structural defects within ER-
345 PM junctions, we reversed the direction of fluorescent tags on Orai1 as well as Stim1 and
346 repeated the experiment in Figure 6A-F. Interestingly, the defect in Stim1 mediated
347 entrapment of Orai1 could be rescued (Supplementary Figure 10A-B) (Figure 6G-J) but
348 SOCE remained significantly inhibited even when Orai1 and Stim1 were co-
349 overexpressed (Figure 6K-L). Taken together, these data show that STX11 binding to
350 resting Orai1 has implications beyond mere co-entrapment of Orai1 with Stim1. STX11
351 depletion did not alter the structure or proximity of junctional ER to the PM and yet
352 reduced SOCE even in cells co-overexpressing Orai and Stim that have been proposed
353 to be sufficient for amplifying CRAC currents in earlier studies [25] [26] [27].
354
355 Defects in the functional entrapment of Orai1 suggest the absence of a necessary
356 molecular transition within Orai1 which precedes its interaction and gating by Stim1. To
357 test whether STX11 induced structural changes within CRAC channel pore subunit,
358 Orai1, we co-expressed Orai1-CFP along with Orai1-YFP in scramble control or STX11
359 depleted HEK293 cells and measured Orai:Orai FRET. We found significantly higher
360 Orai1:Orai1 FRET in STX11 depleted resting cells even in the absence of ectopically
361 expressed Stim1. (Figure 7A). We have previously shown that store-depletion induces
362 on-site assembly of Orai1 dimers into oligomers [14]. Notably, store-depletion induced a
363 similar level of increase in Orai1:Orai1 FRET in scramble control cells. To confirm these
364 findings, we performed acceptor photobleaching analysis on Orai1-CFP (donor), Orai1-
365 YFP (acceptor) co-expressing HEK293 resting cells where we had stably knocked down
366 the expression of endogenous Orai1 and Stim1. Although the trends were largely similar,
367 the differences in Orai1:Orai1 FRET were much more significant in these cells (Figure
368 7B-C). These data demonstrate a previously unsuspected, novel, molecular transition in
369 Orai1 necessary for CRAC channel activation, which we define as 'priming'. Further,
370 these data show that priming precedes the interaction of Orai1 with Stim1 in ER-PM
371 junctions. To determine whether 'priming' simply induced a structural change or facilitated
372 correct assembly of Orai1 multimers, we expressed Flag-Orai1 in control or STX11

373 depleted resting cells, mechanically lysed to isolate membranes, crosslinked Orai1
374 oligomers using BS3 and resolved using SDS-PAGE (Figure 7D) (Supplementary Figure
375 11A). We found a greater percentage of higher order oligomers in STX11 depleted cells
376 suggesting stoichiometric changes (Figure 7E) (Supplementary Figure 11A).
377
378 Increasing the density of Stim1 has been earlier proposed to bypass the
379 requirements for accessory factors in SOCE. To determine whether increasing the levels
380 of Stim1 could compensate for STX11 depletion, we expressed Orai1 tethered to two
381 Stim-Orai activating region (SOAR) domains of Stim1 and GFP (Orai1-S-S-GFP)
382 (Supplementary Figure 11B-C) in HEK293 cells. Orai1-S-S-GFP has been previously
383 shown to constitutively activate Orai1 [23]. In STX11-depleted Orai1-S-S-GFP expressing
384 cells, the magnitude of calcium entry was significantly smaller (Supplementary Figure
385 11D-E). To determine whether reduced calcium entry resulted from a defect in the ability
386 of SOAR to bind Orai1, we expressed YFP-CAD, in control or STX11 depleted Orai1-CFP
387 expressing HEK293 cell line (Figure 7F). Quantification of PM localized YFP-CAD as a
388 fraction of total CAD showed no defect in STX11 depleted cells (Figure 7F). Yet, as seen
389 with Orai1-S-S-GFP, constitutive calcium entry was significantly reduced (Figure 7G-H).
390 We next expressed a constitutively active H134S mutant of Orai1 (Supplementary Figure
391 11F) as it harbors an open pore and the C-terminal cytosolic tails of Orai1 are unlatched,
392 pointing towards the cytosol [28]. Remarkably, expression of H134S Orai1 completely
393 restored constitutive calcium influx in STX11 depleted cells (Figure 7I-J). To further
394 establish whether binding with STX11 induces straightening of Orai1 tails or molecular
395 transitions within transmembrane helices, we expressed in STX11 depleted cells the
396 constitutively active ANSGA (261-265) mutant of Orai1 (Supplementary Figure 11G),
397 which harbors 4 consecutive mutations in the Orai1 C-terminus resulting in the
398 straightening of the C-terminal tail along with constitutive activation of CRAC currents
399 [29]. The constitutive calcium entry in STX11 deficient Orai1 ANSGA mutant expressing
400 cells was significantly suppressed (Figure 7K-L). Taken together, these data show that
401 STX11 induces a molecular switch in the pore-forming subunit, Orai1, which precedes
402 and primes it for optimal on-site assembly into multimers and subsequent gating by Stim1.
403 Such SNARE dependent priming of Orai1 is crucial and cannot be compensated by

404 merely increasing the density of Stim proteins bound to Orai or by introducing mutations
405 that alter the orientation of Orai1 tails *in vivo*. The proposed models depicting unprimed
406 and primed Orai1 (Figure 8A) and its role in T cell function (Figure 8B) are shown.
407
408 Q-SNAREs are often found in complex with other SNAREs such as SNAP23/25/29
409 in target membranes. Some previous studies have implicated the complex of SNAP23/25
410 and STX1A in the regulation of specific ion channels [30, 31]. The three SNAPs,
411 SNAP23/SNAP25/SNAP29 are each capable of contributing two SNARE domains to the
412 *trans*- and *cis*-SNARE complex. RNAi mediated depletion of SNAP23/SNAP25/SNAP29
413 did not show a significant reduction in SOCE of HEK 293 cells (Supplementary Figure
414 12A-C). To determine whether SNAP23/SNAP25/SNAP29 might still form a part of the
415 STX11:Orai complex to regulate SOCE, we co-expressed myc-tagged Orai1 with
416 untagged SNAPs and performed respective co-IPs. We did not find any interaction
417 between either of the three SNAPs and Orai1 (Supplementary Figure 12D). Similar
418 studies were performed by co-expressing YFP-Stim1 and the three myc-tagged SNAPs.
419 Again, no interaction was found between any of the SNAPs and Stim1 (Supplementary
420 Figure 12E). These data show that, unlike in the case of vesicle fusion, STX11 does not
421 collaborate with SNAP23/SNAP25/SNAP29 in the regulation of SOCE.
422
423 FHLH is a heterogeneous immune disorder where diverse genes such as *Prf1*,
424 *STX11*, *UNC13D*, *Munc18-2*, *MAGT1, XIAP, LYST, AP3B1, RAB27A*, *ITK*, amongst
425 several others, are broadly grouped together based on disease symptoms, although the
426 age of onset and severity varies across the spectrum [32, 33]. Congenital
427 immunodeficiency involving defects in the CTL and NK cell cytotoxicity appear to be the
428 common factors underlying the development of FHLH, although the individual pathways
429 involved are highly diverse. Using shRNA, we screened 6 additional genes, *Perforin1*,
430 *RAB27A*, *UNC13D* and *Munc18-2*, *Synaptotagmin11* and *13*, that have been either
431 associated with vesicle fusion or routinely grouped together with STX11 in diagnosing
432 FHLH (Supplementary Figure 13). SOCE was not affected by depletion of most genes.
433 Future studies will evaluate the role of others.
434

435 **Discussion:**

436

437 CRAC channels conduct a small, highly specific calcium current in response to the
438 depletion of intracellular calcium stores. According to the prevailing view, Orai multimers
439 reside in the PM and depend on the ER resident store sensor, Stim, for all structural
440 transitions leading up to their activation [10]. Unlike other ion channels, the process of
441 activation of CRAC currents is exceptionally slow. For instance, following break-in or
442 store-depletion, on average, it takes ~5 minutes for Stims to cluster in the ER-PM
443 junctions and for measurable CRAC currents to flow from Orai1. During this time, Stims
444 undergo intramolecular transitions and slowly trap and gate freely diffusing Orai. It is,
445 therefore, believed that no molecular transitions take place within the pore forming
446 subunit, Orai, until its entrapment by Stim in the ER-PM junctions.

447

448 We have shown that in STX11 deficient cells, the basal Orai:Orai FRET is
449 significantly higher even in the absence of Stim1 or store-depletion. These data establish
450 that Orai1 undergoes a, hitherto unrecognized, SNARE dependent molecular transition
451 which precedes trapping and gating by Stim1. We have earlier shown that store-depletion
452 induces dynamic on-site assembly of Orai1 dimers into oligomers [14]. In STX11 depleted
453 resting cells, the ~25-50% increase over basal Orai:Orai FRET largely results from a
454 change in the oligomerization of Orai1 because the proportion of BS3 crosslinked Orai1
455 oligomers was also found to be shifted towards higher molecular weight. It is likely,
456 though, that a change in the overall conformation of Orai1 protomers facilitated the
457 change in store-dependent Orai assembly and contributed to the overall change in
458 Orai:Orai FRET.

459

460 The change in Orai:Orai FRET induced by STX11 depletion not only persisted but
461 increased in Orai1, Stim1 double deficient cells. Furthermore, STX11 bound a region of
462 Orai1 C-terminus that has been previously shown to bind Stim1. Therefore, our data
463 suggest that STX11 induced molecular transitions in Orai are independent of and precede
464 its association and clustering by Stims. Because tagging of STX11 with fluorescent tags
465 on either end results in mis localization and degradation, our study could not demonstrate

466 the real-time removal of STX11 from the Orai1- C-terminus to allow for Stim1 binding in
467 live cells. It is also unclear whether binding or removal of STX11 induced the proposed
468 molecular transition defined as 'priming' of Orai1. Further, it remains to be determined
469 whether STX11 removal is actively induced by an additional chaperone or passive
470 displacement from the formation of relatively higher avidity oligomeric associations
471 between Orai1:Stim1 in ER-PM junctions. Future studies will be able to systematically
472 evaluate each of these possibilities.
473
474 We have shown that the C-terminal cytosolic tail of Orai1 directly couples with
475 STX11 in resting cells. Although binding appeared reasonably strong in co-IPs,
476 STX11:Orai1 interaction appeared somewhat weak in pull-downs. This is likely due, in
477 part, to the instability of purified His-STX11 in solution which necessitated shorter co-
478 incubation times during pull-down assays. Instability could arise from the absence of a
479 stabilizing co-chaperone, such as one of the known binding partners of SNAREs [34] [35]
480 or membranes to which STX11 attaches in lives cells *via* its C-terminal cysteines [21].
481 Together, these factors appear crucial for the stabilization of purified STX11 *in vitro*.
482
483 Stim1 binds the N- as well as the C-terminus of Orai1 but their individual relevance
484 in the trapping *versus* gating of Orai1 remains unclear [36]. Though crucial for trapping
485 and gating, Orai1 tails were missing from early structures of *Drosophila* Orai [28]. A
486 previous NMR structure suggested that C-terminal tails of two adjacent Orai1 subunits,
487 bend, pair with each other in an antiparallel fashion and sit closely apposed to PM [37].
488 However, in recent structures of constitutively active H134 mutant Orai, the C-terminal
489 tails were found to orient away from the membrane [28]. In STX11 depleted cells,
490 switching the CFP-tag from the Orai1 N- to the C-terminus could rescue its clustering but
491 not gating by Stim1. Furthermore, STX11 depletion inhibited the constitutively active
492 ANSGA mutant of Orai1 [29], where the tails of Orai1 are proposed to be constitutively
493 unlatched. These data essentially reinforce our conclusions that STX11 induced
494 molecular shifts encompass Orai1 transmembranes.
495

496 Using Fura-2 imaging assays in STX11 depleted cells, we have conclusively
497 established that STX11 is necessary as well as limiting not only in live and unperturbed
498 HEK, U2OS, Jurkat and primary T cells but also HEK293 cells co-overexpressing Orai1
499 and Stim1. Previous whole cell patch clamp analysis of HEK293 cells co-overexpressing
500 Orai1 and Stim1 showed up to 50-100-fold amplification of CRAC currents whereas Fura-
501 2 based imaging of live cells routinely shows only 2-fold amplification [25] [26] [27]. The
502 patch clamp studies performed on Stim, Orai over-expressing cells are often extrapolated
503 to conclude that all other accessory factors that have since been identified are
504 unnecessary for native CRAC currents. A major problem with this interpretation is that
505 even though amplification of CRAC currents was shown, none of the previous patch
506 clamp studies established whether the higher currents resulted from a greater number of
507 active channels or unchecked conductance per channel by performing single channel
508 recordings. The fact that recording of I_{CRAC} in the whole cell configuration involves use of
509 20mM extracellular calcium and dialysis of cells with high concentrations of BAPTA, a
510 fast calcium chelator, the calcium dependent inactivation of CRAC channels, a key
511 mechanism of regulation of I_{CRAC} magnitude in live cells is disrupted. Furthermore,
512 hyperpolarizing potentials and voltage clamping used to record CRAC currents prevents
513 the progressive depolarization of cells due to influx of cations which would otherwise
514 dampen the driving force for CRAC currents in intact cells. Given these limitations, Fura-
515 2 assays offer a more realistic and physiological reflection of SOCE amplitudes in live
516 cells as they allow for these regulatory mechanisms, which are necessary for the
517 regulation of native currents to be still operational. While patch clamp remains a direct
518 method of verification of CRAC currents, exercising logic in extrapolation of amplitudes
519 of I_{CRAC} using patch clamp is imperative for the field to move forward.
520
521 Most human mutations in the *STX11* coding region result in the complete loss or
522 severe depletion of STX11 protein levels [21]. The FHLH4 disease, therefore, results from
523 reduced STX11 expression in most reported patients. Targeted mutagenesis of the
524 STX11:Orai1 interface lining residues based on the AlphaFold 3 model, however, didn't
525 destabilize or mis-localize either N147A_E150A STX11 or
526 R289A_E272A_E275A_E278A Orai1 and yet both mutants showed reduced binding to

527 their respective wildtype counterparts. Importantly, the R289A_E272A_E275A_E278A
528 mutant of Orai1 retained the ability to bind Stim1.
529
530 In addition to the established cytolytic defects in FHLH4 T cells, for the first time,
531 we have shown that STX11 deficient, FHLH4 T cells harbor a severe defect in store-
532 operated calcium signaling and IL-2 gene expression. Our data strongly suggest that
533 SOCE defects significantly contribute to FHLH4 disease progression *via*, as well as
534 independent of, exocytotic/ degranulation defects. We propose that design and early
535 administration of CRAC channel agonists could potentially provide an alternative to
536 immunosuppressants and bone marrow transplants for FHLH4 patients.
537
538 In summary, we have shown that binding to a Q-SNARE, STX11, provides an on-
539 site molecular switch in the CRAC channel pore, Orai1, necessary for its optimal
540 assembly and function. We suggest that ion channel priming is a novel, direct and primary
541 role of specific SNAREs. In accordance with this hypothesis, early SNARE-like proteins
542 have been found in bacteria, which lack an endomembrane system but express a variety
543 of ion channels [38-40]. SNAREs are now thought to have evolved from a common
544 archaeal precursor found in the genomes of Asgard and members of *Legionella* [41].
545
546
547
548
549
550
551
552
553
554
555
556
557

558 **Materials and Methods**

559

560 **Plasmid constructs and transfection**

561 Stim1 CAD was sub-cloned in eYFPC1 vector after amplification from YFP-Stim1 plasmid
562 to generate YFP-CAD. pLKO.1, psPAX2 and pMD2.G were purchased from Addgene.
563 pLKO.1 cloned shRNA sequences targeting the genes of interest, were either purchased
564 from Horizon Discovery, UK or designed and cloned in-house using the Broad Institute
565 portal (https://portals.broadinstitute.org/gpp/public/gene/search). Full-length human
566 STX11 was cloned from human cDNA prepared from HEK293 cells and subcloned into
567 pcDNA3.1(+), pcDNA/4TO/Myc-HisA (Invitrogen, Grand Island, NY), pMSCV-IRES-
568 mcherry (Addgene), pEF1alpha-IRES (Clontech) and pET28b vector [16] with an N-
569 terminal 6XHis-tag. The fragments of STX11 were cloned in pET28b vector with an N-
570 terminal 6xHis tag for expression in *E. coli*. HA tag was inserted between H30 and G31
571 in STX11 cloned in pMSCV-IRES-mCherry construct using PCR. H134S and ANSGA
572 mutants of Orai1 were generated using site directed mutagenesis and PCR, respectively.
573 The fragments of Orai1 (1-87, 1-47, 48-103, 256-301 and 272-292) were amplified from
574 full length constructs and cloned into pMAL-c5X vector (New England Biolabs), in-frame
575 with MBP protein coding sequence, as described previously [16]. SNAP23, SNAP25 and
576 SNAP29 cDNA cloned in pCMV-Sport6.1 vectors were purchased from Dharmacon and
577 subcloned into pcDNA4/TO/Myc-HisA. SNAP23 was subcloned in pMAL-c5X vector in-
578 frame with MBP. All plasmid DNA transfections in human cell lines and primary cells were
579 done using Lipofectamine 2000 (Invitrogen)/ Lipofectamine 3000 (Invitrogen) or Amaxa
580 nucleofection kit (Lonza, Basel, Switzerland) respectively, as per manufacturer's protocol.

581

582 **Cell Lines**

583 Lentiviral shRNA transduction experiments were performed in HEK293, U2OS or Jurkat
584 (ATCC, Manassas, VA) cell lines cultured in low glucose DMEM (Hyclone, Logan, UT) or
585 RPMI (Hyclone) respectively, with 5-10% fetal bovine serum (Hyclone), 1X Penicillin
586 Streptomycin, and GlutaMax (Gibco, Grand Island, NY). Stable cell lines generated using
587 HEK293 and U2OS parent lines have been described previously [9]. HEK293-FT cell line
588 was cultured in high glucose DMEM with 10% FBS and 10mM HEPES, 1X Penicillin

589 Streptomycin, 1X GlutaMax and 1X non-essential amino acid and transfected with the
590 appropriate plasmids to generate viral supernatants. All cell lines were tested for
591 mycoplasma contamination twice every year and found to be negative.
592
593 **Antibodies and Reagents**

Antibodies/Reagents	**Source and Cat no**	**Dilution/ Conc.**
Mouse anti-myc (9E10)	Abcam #ab32	1:1000
Mouse anti-myc (9E10)	Culture supernatant, in house	1:1000
Rabbit anti-SNAP23	SYSY#111203	1:1500
Mouse anti-SNAP25	SYSY#111011	1:1500
Rabbit anti-SNAP29	SYSY#111303	1:1500
Rabbit anti-GFP	Invitrogen#A11122	1:2500
Rabbit anti-flag	Sigma#F7425	1:1600
Mouse anti-flag (M2)	Sigma#F3165	1:1500
Mouse anti-6X His	Invitrogen #MA1-135	1:2000
Rabbit anti-Stx11	Sigma#SAB4301593	1:1000
Mouse anti-NFATc2 (4G6-G5)	Santacruz#7296	1:500
Rabbit anti-NFAT1	Cell Signaling Technology #4389	1:200
Goat anti-Lamin B (M-20)	Santacruz#6217	1:500
Rabbit monoclonal anti-HA	CST#3724S	1:1000
Alpaca VHH anti-rabbit AF488	Jackson #611-544-152	1:400 (1.375μg/ml)
DAPI	Invitrogen #D1306	2μg/ml
Rabbit anti-Stx11	SySy #110113	1.67μg/ml
Rabbit anti-Stx11	Invitrogen #PA5-50800	1:2000
Goat anti-rabbit A647	Invitrogen #A-21245	1:800
Rabbit anti-Stx11	Proteintech #13301-1-AP	0.3μg/ml
Donkey anti-rabbit A647	Jackson #711-605-152	1:800

HRP GAPDH	Sigma #G9295	1:40000
HRP Donkey anti-Rabbit	Jackson #711-035-152	1:50000
HRP Donkey anti-Mouse	Jackson #715-035-151	1:50000
Purified Human IL-2	BD #555051	1 μg/ml
Purified Human IL-2 Biotin	BD #555040	1 μg/ml
Streptavidin HRP antibody	Jackson #016-030-084	0.1 μg/ml
Ultra-LEAF Purified anti-human CD3	Biolegend #317326	5-10μg/ml
Ultra-LEAF Purified anti-human CD28	Biolegend #302934	2μg/ml
Ultra-LEAF Purified anti-human CD49d	Biolegend #304340	2μg/ml
PE anti-human CD107a (LAMP-1)	Biolegend #328608	1:50
APC anti-human CD8 antibody	Biolegend #344722	0.5μg/ml
Fura-2-AM	Invitrogen #F1221	1μM
Thapsigargin (TG)	Sigma #T9033-1MG	1μM
Polybrene (Hexadimethrine-bromide)	Sigma #107689-10G	8μg/ml
NE-PER kit	Thermo #78833	
Protein A/G Mag Sepharose xtra	Cytiva #28967056/66	
Protein A/G 4 Fast Flow Sepharose	Cytiva #17528001	
Protease Inhibitor Cocktail (Mammalian)	Sigma #539134	
Protease Inhibitor Cocktail (Bacterial)	Calbiochem #539132	
Talon Beads	Takara #635502	
Dextrin Sepharose Beads	Cytiva #28935597	

HEPES	Sigma #H3375-100G	
Lipofectamine 2000	Thermofisher #11668019	
Lipofectamine 3000	Thermofisher #L3000001	
Lemo21(DE3) *E.coli.* cells	NEB #C2528J	
IPTG	Himedia#MB072-10G Sigma #16758-10G	
Sarkosyl (N-lauroylsarcosine sodium salt)	Sigma #L9150-50G	
Lysozyme	Sigma #62970-5G-F	
DNaseI Recombinant RNase-free	Roche #04716728001	
PMA (Phorbol Myristate Acetate)	Sigma #P8139	20-50ng/ml
Ionomycin	Sigma #407952	1μM
Human IL-2 protein	Acro Biosystems #H5215	50ng/ml
Lectin from *Phaseolus vulgaris* (PHA)	Sigma #L8754	2μg/ml
Retronectin	Takara #T100B	20μg/ml
RNeasy Plus Mini kit	Qiagen#74134	
QIAshredder	Qiagen#79654	
Superscript IV	ThermoFisher#18091300	
Qubit ssDNA Assay kit	ThermoFisher# Q10212	
Human STX11 TaqMan probe (FAM-MGB)	ThermoFisher# Hs00186823_m1	
Human Beta Actin TaqMan probe(FAM-MGB)	ThermoFisher# Hs01060665_g1	
Human IL2 Taqman probe (FAM-MGB)	ThermoFisher# Hs00174114_m1	
Paraformaldehyde	Electron Microscopy Sciences #157-8	

Bovine Serum Albumin	Jackson #001000173	
Luria Bertini Broth	Himedia #M1245	
HBSS	Sigma #H8264	
Terrific Broth	Sigma #T9179	
Alexa fluor 647 conjugated Alpha Bungarotoxin	Invitrogen #B35450	1μg/ml
HRP rabbit anti-GFP	Invitrogen #A10260	
HRP Goat anti-rabbit Fc	Jackson #111-035-008	1:50,000
Ampicillin	Sigma #A0166-5G	100ug/ml
Kanamycin	Sigma #K1876-1G	50ug/ml
Chloramphenicol	Sigma #C 0378-5G	100ug/ml
30% Acrylamide:Bis Solution (29:1)	Biorad #1610156	
DTT (Dithiothreitol)	Biorad #1610611	
0.05% Trypsin-EDTA	Gibco #25300054	
100X Penicillin Streptomycin	Sigma #P4333-100ML	
Puromycin	Gibco #A11138-03	
Pluronic F-127 (20% solution in DMSO)	Invitrogen #P3000MP	0.02%

Lentiviral transductions

For the generation of lentiviral supernatants, shRNAs cloned in pLKO.1 were co-transfected with psPAX2 packaging and pMD2.G envelope plasmids into HEK293-FT cells using the calcium phosphate method of transfection. 48- and 72-hours post-transfection, viral supernatants were collected, pooled and stored at -80°C till further use. For transduction of HEK293 and Jurkat cells, 0.1 million cells were plated in 6- or 24-well plates either the day before (HEK293) or the same day (Jurkat). Viral supernatants were added to the cells along with 8ug/ml polybrene and cells were spun at 2500 RPM, 30°C for 90 mins. 24 hours or 48 hours post-spinfection, Puromycin was added at a final

605 concentration of 1ug/ml to HEK293 and Jurkat cells, respectively. Cells were analyzed 3-
606 5 days post transduction.
607
608 **Immunocytochemistry and confocal imaging**
609 For STX11 localization, resting or store-depleted (1μM Thapsigargin) WT HEK293 or
610 HEK293 cells stably expressing Orai1-YFP were either plated in 6 well plates and
611 spinfected with viral supernatants generated from pMSCV-STX11(HA)-IRES-mCherry,
612 pMSCV-IRES-mCherry (empty vector control) or plated in carbon coated, glow
613 discharged 35mm glass bottom dishes (IBDI) and transfected with pEF1alpha-STX11-
614 IRES-mCherry. 24 hr post-spinfection, cells were plated in 35mm glass bottom dishes.
615 For immunolabelling, cells were washed with Ringer's buffer, fixed with 4% PFA and
616 blocked with 3% BSA containing 0.1% NP40 for 1.5 hrs. Post-fixation and
617 permeabilization, cells were incubated either with anti-HA (CST) or rabbit anti-Stx11
618 (SySy/ Proteintech) primary antibodies O/N at 4°C, washed and incubated with either
619 Alpaca VHH anti-rabbit AF488, donkey anti-rabbit A647 or goat anti-rabbit A647
620 secondary antibodies for 1 hour at room temperature (RT). Cells were counter stained
621 with DAPI for 10 min at RT and imaged using Olympus FV3000 laser scanning confocal
622 microscope. Images were acquired sequentially using the following parameters: DAPI
623 (DM405/488 dichroic, 405nm excitation, 430-470nm emission); anti-HA Alexa488
624 (DM405/488, 488nm excitation, 500-590nm emission); STX11 (DM405/488/561/640,
625 640nm excitation, 650-750nm emission); Orai1-YFP (DM405/488/561/640, 488nm
626 excitation, 521-591nm emission); CFP-Stim1 (DM405-445/514/594, 405nm excitation,
627 448-510nm emission). For STX11-N147A-E150A mutant, HEK293 cells were spinfected
628 with viral supernatants and imaged as described above where WGA (Wheat germ
629 agglutinin) conjugated with Alexa 488 was used to mark plasma membrane.
630
631 **Quantification of Orai1 and Stim1 intensities inside/outside ER-PM puncta**
632 HEK293 cells stably expressing Orai1-YFP with CFP-Stim1 or CFP-Orai1 with Stim1-YFP
633 were plated in 6 well plates and transduced with scramble or STX11 shRNA. 48hr post
634 transduction, cells were trypsinized and plated in carbon coated 35mm dishes. Images
635 were acquired using a TIRF microscope setup described before [14]. Briefly, resting cells

636 were imaged first and positions were marked. Store-depleted images were acquired after
637 incubation with 1 μM Thapsigargin (TG) and 10mM EGTA for ~6 mins. Analysis was done
638 using Otsu local thresholding in ImageJ software. Stim1 and Orai1 intensity (AU) and area
639 μm^2 values obtained from the analysis were plotted using Origin software.
640
641 **Orai:Orai FRET**
642 Scramble and STX11 shRNA transduced HEK293 cells were plated on freshly carbon
643 coated, glow discharged 35mm glass bottom dishes (IBDI) and transfected with 0.5 μg
644 each of Orai1-CFP and Orai1-YPF plasmid DNA using Lipofectamine 3000. 16 hours post
645 transfection, co-transfected cells were imaged using PlanApoN 60XO/1.42 NA
646 objective with Olympus FV3000 laser scanning microscope. Orai1-CFP, Orai1-YFP and
647 FRET images were acquired with the following excitation laser and emission bandwidth
648 parameters using DM405-445/514 dichroic mirror: CFP Ex-405nm Em-460-630nm; YFP
649 Ex-514nm Em- 530-630nm; FRET Ex-405nm, Em-530-630nm. ROIs representing the
650 plasma membrane rim were drawn around each cell, followed by local thresholding using
651 Bernsen's algorithm in Fiji software to generate an image mask which was applied to
652 CFP, YFP, FRET images to extract mean intensity values. The background subtracted
653 mean intensities of FRET (I_{FRET}), CFP (I_{Donor}) and YFP($I_{acceptor}$) images were measured
654 for each cell. Cells singly expressing Orai1-CFP or Orai1-YFP only were used as CFP
655 donor or YFP acceptor channel bleed-through (BT) controls. The BT was calculated using
656 the following formula:
657 $\mathrm{BT_{Donor}} = \frac{\mathrm{I_{FRET}}}{\mathrm{I_{Donor}}}$ when the Orai1-CFP donor alone is expressed,
658 $\mathrm{BT_{acceptor}} = \frac{\mathrm{I_{FRET}}}{\mathrm{I_{acceptor}}}$ when the Orai1-YFP acceptor alone is expressed.
659
660 FRET and NFRET percentage was calculated by subtracting the contributions of CFP
661 and YFP bleed through from the FRET signal using the following:
662 $$FRET = I_{FRET} - (BT_{Donor} * I_{Donor}) - \left(BT_{Acceptor} * I_{Acceptor}\right)$$
663

664 $$NFRET\% = \left(\frac{FRET}{\sqrt{\left(I_{Acceptor} * I_{Donor}\right)}} \right) * 100$$

665

666 **Acceptor Photobleaching**

667 Scramble and STX11 shRNA transduced, Orai1, Stim1 double knockdown HEK293 cells
668 where were plated on Poly-D-Lysine coated glass bottom dishes (Cellvis) and transfected
669 with 0.5 ug DNA each of Orai1-CFP and Orai1-YPF using Lipofectamine 2000. 16 hours
670 post transfection, co-transfected cells were imaged using PlanApoN 60XO/1.42 NA
671 objective with Olympus FV3000 laser scanning microscope. Images were acquired with
672 the following excitation laser and emission bandwidth parameters using DM405-445/514
673 dichroic mirror: CFP Ex-405nm Em-460-508nm; YFP Ex-514nm Em- 530-630nm, with
674 4% offset. The pre bleach images of Orai1-CFP (the donor) and Orai1-YFP (the acceptor)
675 were captured, sequentially. This was followed by bleaching of the acceptor, Orai1-YFP,
676 using 100% 514 laser power for 2 mins and then acquiring the donor and acceptor images
677 post bleach. ROIs were drawn around the cell periphery using the Orai1-CFP image.
678 Local thresholding was performed using Bernsen's algorithm to generate binary masks,
679 which were then applied to the CFP images to measure mean intensities. The background
680 subtracted mean intensities of CFP images were measured for each cell and the FRET
681 efficiencies were calculated as follows: E (%) = (1 -I_{before}/I_{after}) *100. I_{before} and I_{after} denotes
682 the average fluorescence intensity of the donor in the plasma membrane before and after
683 acceptor photobleaching.

684

685 **Alpha-bungarotoxin binding assay**

686 U2OS cell line stably expressing Orai1-BBS-YFP construct has been described
687 previously[14]. Briefly, Orai1-BBS-YFP expressing U2OS cells were either transduced with
688 scramble shRNA/ STX11 shRNA/ pMSCV-IRES-mcherry (EV) or pMSCV-STX11-IRES-
689 mcherry. Transduced cells were trypsinized either 3-4 days post-transduction or 48 hour
690 post-transduction (in the case of pMSCV), centrifuged and labelled on ice with AF647
691 conjugated alpha-bungarotoxin (1μg/ml) containing 2% FBS in 1X HBSS for 30 mins.
692 Following this, cells were washed with HBSS and fixed with 4% PFA (~20 min at RT).

693 Samples were run using Cytoflex FACS analyzer (Beckman Coulter) and data were
694 analyzed using Flow Jo software.
695
696 **Validation of STX11 knockdown using qPCR**
697 Scramble and STX11 shRNA treated HEK293 cells were trypsinized, counted and equal
698 number of cells were used for lysis. The lysates were homogenized using QIA shredder
699 columns (Qiagen) and RNA isolation was done using RNeasy Plus Mini kit (Qiagen). Total
700 RNA isolated from both the groups was used for cDNA synthesis using oligo dT primers
701 and Superscript IV as per manufacturer's guidelines. The concentration of synthesized
702 cDNA was estimated using Qubit ssDNA assay kit and STX11 TaqMan probes were used
703 to perform the qPCR using LightCycler 96 (Roche). Beta-actin was used as housekeeping
704 control.
705
706 **Single cell Ca^{2+} imaging**
707 Cells were plated in carbon-coated glass bottom dishes (one day prior or 30 mins before
708 the assay for HEK293 and Jurkat T cells respectively) and loaded with 1μM Fura-2 AM
709 dye in HBSS ($CaCl_2$ 1.8mM, KCl 5.36mM, $MgSO_4$ 0.81mM, NaCl 136.89 mM, Na_2HPO4
710 0.335mM, D-Glucose 5.55mM) for 30 mins, at 37°C in the dark. After incubation, cells
711 were washed and incubated in Ringer's buffer (135mM NaCl, 5mM KCl, 1.8mM $CaCl_2$,
712 1mM $MgCl_2$, 5.6mM Glucose, 10mM HEPES) for an additional 10 mins, washed and
713 imaged in Ringer's buffer or Calcium-free Ringer's buffer (135mM NaCl, 5mM KCl, 1mM
714 $MgCl_2$, 5.6mM Glucose, 10mM HEPES at pH7.5), as indicated. Olympus IX-71 inverted
715 microscope equipped with a Lamda-LS illuminator (Sutter Instrument, Novato, CA), Fura-
716 2 (340/380) filter set (Chroma, Bellows Falls, VT), a 10X 0.3NA objective lens (Olympus,
717 UPLFLN, Japan), and a Photometrics Coolsnap HQ2 CCD camera was used to capture
718 images at a frequency of ~1 image pair every 2 or 4 seconds interval. Data were acquired,
719 analyzed and plotted using MetaFluor (Molecular Devices, Sunnyvale, CA), Microsoft
720 Excel, and Origin softwares. Approximately 30-40 cells were imaged per group in each
721 experiment unless otherwise stated. Mean SOCE ± SE for each experiment was
722 calculated from three independent experiments where the maximum value of the

723 scramble shRNA group (amongst the three experiments) was set at 100% and the relative
724 responses of other scr and STX11 shRNA groups were normalized w.r.t it.
725 For constitutive calcium influx assay, shRNA treated HEK293 cells were either
726 transfected or nucleofected with Orai1-S-S-EGFP, Orai1(H134S)-YFP or Orai1(ANSGA)-
727 YFP and ~12-14 hour post transfection (~4-5 hour post nucleofection), cells were loaded
728 with Fura-2 AM, washed and imaged in Ringer's buffer with 0 mM calcium to acquire
729 baselines and 2 mM calcium thereafter. To measure CAD induced constitutive calcium
730 influx, Orai1-CFP expressing stable HEK293 cells were nucleofected with YFP-CAD and
731 analyzed ~4 hour later as described above. To identify cells expressing Orai1 mutants
732 and fusion proteins in the plasma membrane, cells were imaged using a 20X 0.7NA water
733 objective lens (Olympus, UApoN340, Japan). Images were acquired at a frequency of ~1
734 image pair every 10 seconds interval to avoid photobleaching and analyzed as described
735 above.
736
737 **Measurement of NFAT nuclear localization by Western blot**
738 Jurkat T cells were transduced with scramble or STX11 shRNA to knock-down STX11 as
739 described above. On day 4 post-transduction, cells were collected, spun down and
740 resuspended in plain RPMI media and rested for 1hr at 37°C. Following this, cells were
741 counted and divided into two equal groups. One group was resuspended in RPMI
742 (unstimulated) and the other in RPMI media containing 1 μM TG + 10 ng/ml PMA (Phorbol
743 Myristate Acetate) (stimulated) and incubated at 37°C for 30 mins. Following incubation,
744 cells were pelleted and the nuclear and cytosolic protein fractions were separated using
745 NE-PER kit according to the manufacturer's guidelines and subjected to SDS-PAGE and
746 western blot using the mouse anti-NFATc2 primary antibody (Santa Cruz) followed by
747 Donkey anti-mouse secondary antibody.
748
749 **Estimation of nuclear translocation of NFAT by immunolabeling**
750 Control and STX11 depleted Jurkat T cells were rested in plain RPMI for ~1 hour prior to
751 the assay. ~100,000 cells per group were plated on freshly carbon-coated coverslips for
752 40 minutes and stimulated for 1 hour at 37°C with 5 μg/ml anti-CD3 antibody, diluted in
753 plain RPMI. Following this, cells were washed and fixed using 4% PFA diluted in 1X PBS

754 for 20 minutes at RT, washed twice and incubated with 30 mM Glycine for 10 minutes at
755 RT. For permeabilization and blocking, cells were incubated with 0.1% Saponin, 3% BSA
756 diluted in 1X PBS for 1 hour at RT, washed and incubated with anti-NFAT primary
757 antibody (anti-NFAT1, CST) at 4°C, overnight. Following primary antibody application,
758 cells were washed with 1X PBS and incubated with anti-Rabbit AF647 secondary
759 antibody for 1 hour, washed and stained with DAPI for 5 minutes followed by additional
760 washes. Images were acquired in the FV3000 confocal microscope using a 100X
761 objective lens. DAPI was used to identify the nuclear area. Nuclear *versus* whole cell
762 (total) NFAT mean intensity ratio was plotted across different groups.
763
764
765 **Whole cell lysates (WCLs), Western blot and Co-immunoprecipitation (Co-IP)**
766 HEK293 cells transfected with the desired plasmids were lysed using buffer containing
767 50 mM Tris-Cl (pH 8.0), 150 mM NaCl, 1% NP-40, 1 mM PMSF, and protease inhibitor
768 cocktail. The whole cell lysates were centrifuged at 21000 g for 15 minutes and
769 supernatants were subjected to SDS-PAGE, and western blot. For immunoprecipitations,
770 lysates were divided into two equal parts. To the first tube, the appropriate anti-mouse or
771 anti-rabbit primary antibody was added and to the second, same amount of the respective
772 IgG control antibody was added. The antibody-lysate mixtures were incubated overnight
773 at 4°C. Following this, Protein A/G Mag Sepharose beads were added and incubated with
774 the antibody-lysate mixtures for 4 hours, washed with the lysis buffer containing 0.1% NP-
775 40, boiled with 1X Laemmli buffer + 120 mM DTT and subjected to SDS-PAGE and
776 western blot analysis. Typically, 1/10th of the whole cell lysate (WCL) was loaded in the
777 input lane of the co-IP blots. The full-length blots pertaining to each figure have been
778 deposited in Zenodo https://doi.org/10.5281/zenodo.19045452.
779
780 ***E. coli* expression and *in-vitro* binding assays**
781 Full-length His_6-tagged Stx11 and truncation mutants were cloned in pET28b, expressed
782 in Lemo21 (DE3) *E. coli* cells and induced with 1 mM IPTG (Isopropyl β- d-1-
783 thiogalactopyranoside) for 14-18 hours at 18°C. The cell pellets were lysed in buffer
784 containing 50 mM Tris-Cl (pH 8.0), 150 mM NaCl, 10% Glycerol, 1 mM PMSF, 1%

785 Sarkosyl, 0.1 mg/ml Lysozyme, protease inhibitor cocktail and sonicated on ice. DNase I
786 was added after sonication and the lysates were further incubated for ~60 minutes before
787 centrifugation at 21000 g for 40 mins. The supernatants were subjected to SDS-PAGE to
788 confirm expression by Coomassie staining and subsequently used for pull-down assays.
789 MBP-tagged Orai1 constructs were expressed in Lemo21 (DE3) *E. coli* cells, induced with
790 0.3mM IPTG (Isopropyl β- d-1-thiogalactopyranoside) for 14-18 hours at 18°C. The cell
791 pellets were lysed in buffer containing 50 mM Tris-Cl (pH 8.0), 150 mM NaCl, 5% Glycerol,
792 1 mM PMSF, 0.1 mg/mL Lysozyme and protease inhibitor cocktail (1:200) and sonicated
793 on ice. DNase I was added after sonication and the lysates were further incubated for ~60
794 minutes before centrifugation at 21000 g for 40 mins. The supernatants were collected
795 and subjected to SDS-PAGE to confirm expression by Coomassie staining and used for
796 pull-down assays. Following lysis, the His_6-tagged Stx11 proteins were purified using
797 Talon Beads and MBP-tagged Orai1 proteins using Dextrin Sepharose/Amylose resin
798 according to the manufacturer's guidelines. For *in-vitro* binding assays, lysates prepared
799 from cells expressing MBP or MBP-tagged Orai1 fragments were incubated with 25 μL
800 Dextrin Sepharose Beads and incubated for 2 hours at 4°C. After incubation, beads were
801 washed thrice and ~50-125 ng of purified His-tagged full length Stx11, His-tagged SNARE
802 or His-tagged H_{abc} domains were diluted in buffer containing 50mM Tris-Cl (pH8), 150
803 mM NaCl, 5% Glycerol and 0.1% NP-40 and added to the beads. Following 1 hour of
804 incubation at 4°C, the beads were washed thrice, re-suspended and boiled in the binding
805 buffer containing 1X Laemmli and 120 mM DTT. The eluate was subjected to SDS-PAGE
806 and Western blot. MBP and MBP-tagged proteins were detected with Ponceau staining,
807 Full length STX11 using Rabbit anti-STX11 primary antibody (Thermo) followed by
808 Donkey anti-rabbit HRP and His-tagged STX11 fragments were detected or mouse anti-
809 6XHis primary antibody (Invitrogen) followed by Donkey anti-mouse HRP secondary
810 antibody.
811
812 **BS3 Crosslinking of Flag-Orai Oligomers:**
813
814 Scramble and STX11 shRNA transduced HEK 293 cells were transfected with Flag-Orai1,
815 harvested, washed, pelleted and subjected to one cycle of snap freeze-thaw. The pellet

816 was resuspended in ice cold lysis buffer (1X HBSS, 1mM PMSF and protease inhibitor
817 cocktail), sonicated for 30 secs (Branson 2510) and mechanically homogenized using
818 dounce homogenizer. The homogenized supernatant was spun at 1500 x g for 10 mins
819 at 4° C, to pellet the cell debris. The supernatant was ultracentrifuged at 105,000 x g for
820 1 hour at 4° C (Optima MAX-XP ultracentrifuge, Beckman Coulter). The membrane
821 fraction pellet was resuspended in lysis buffer and re-homogenized using dounce
822 homogenizer. The protein concentration was estimated using BCA assay and BS3 cross-
823 linker was added to the resuspended membranes, at a final concentration of 1mM, and
824 incubated for 30 mins at room temperature. BS3 was quenched using 50mM Tris-HCl pH
825 7.5 for 15 mins at room temperature, followed by addition of 1X Laemmli and 100 mM
826 DTT and incubation at 37° C for 10 mins. The samples were resolved using 4-15%
827 gradient SDS-PAGE and subjected to Western blot using anti-Flag antibody.
828
829 **Quantification of Flag-Orai oligomers using Western blot:**
830
831 Equal size ROIs were drawn over corresponding protein bands of same size, using
832 ImageJ. The total intensity of each band was measured by calculating the area under the
833 intensity curve and its relative proportion was calculated by dividing the raw intensity of
834 each band by the sum of intensities of all the bands in the respective lanes.
835
836 **qPCR to estimate gene expression in Jurkat T cells**
837 Scramble (scr) and STX11 shRNA treated Jurkat T cells were rested for ~1 hour prior to
838 the assay, stimulated with soluble anti-CD3 (5-10 μg/ml) for 3 hours and washed with
839 HBSS. Total RNA was isolated using RNeasy Mini kit as per manufacturer's instructions.
840 cDNA was synthesized using random hexamers and Invitrogen Superscript IV kit and
841 quantified using Qubit ssDNA assay. Taqman probes for IL-2 and beta-actin
842 housekeeping control were used for performing the qPCR in triplicates. Data analysis was
843 done by calculating the double delta C_t values.
844
845 **EIA to measure IL-2 levels in supernatants of Jurkat T cells**

846 Scramble (scr) and STX11 shRNA treated Jurkat T cells were stimulated with plate-
847 coated anti-CD3 (10 μg/ml) and the culture supernatants were collected at 12 and 24 hour
848 post-stimulation. EIA plates were coated with purified mouse anti-human IL-2 capture
849 antibody (1 μg/ml) overnight at 4°C, washed with 0.05% PBST and blocked with 2% BSA
850 for 2 hours. After blocking, the plates were incubated with the culture supernatants for 2
851 hours at RT, washed and incubated with the detection antibody (Biotin mouse anti-human
852 IL-2, 1 μg/ml) for 2 hours. After washing, Streptavidin HRP (0.1 μg/ml) followed by TMB
853 reagent were added. 250 mM HCl was added to stop the reaction and absorbance was
854 measured at 450 nm.
855
856 **Isolation and culture of human PBMCs**
857 Whole blood freshly collected in Heparin or Citrate Phosphate Dextrose Adenine (CPDA)
858 solution was subjected to density gradient centrifugation using Ficoll-Paque PLUS media.
859 The buffy coat was separated, washed twice with HBSS and cultured with IL-2 (50 ng/ml).
860 Cells were stimulated once per week with PHA (2 μg/ml) for 72 hours and rested in IL-2
861 for the remaining 72-96 hours. Unless specified, all the assays were performed following
862 24-48 hours of rest, post stimulation.
863
864 **Isolation of genomic DNA and sequencing**
865 Genomic DNA was extracted from PBMCs using Phenol-Chloroform-Isoamyl alcohol.
866 STX11 genomic region flanking the mutation was PCR amplified using primers: 5'
867 Forward -CATGCACGACTACAACCAGGC and 3' Reverse -
868 GGGACAGCAGAAGCAGCAGAGGG. The resulting PCR products were separated on
869 2% agarose gel, excised and extracted using the Macherey-Nagel Nucleospin columns
870 and subjected to Sanger sequencing using the 5' Forward PCR primer to confirm the
871 mutation.
872
873 **Measurement of SOCE in human PBMCs**
874 PBMCs in culture were washed, rested and allowed to adhere to freshly carbon-coated
875 (IBDI) dishes for 1 hour in plain RPMI at 37°C. The cells were washed with HBSS and
876 incubated with 1 ml of 1 μM Fura-2-AM diluted in Ringer's buffer for 40 minutes, washed

877 and incubated for an additional 10 minutes to allow de-esterification of the dye. The assay
878 was started with 1 ml of Calcium free Ringer's buffer in the imaging dish and images were
879 captured every 4 seconds. After capturing the baseline for ~60 seconds, stores were
880 depleted by the addition of 1 μM Thapsigargin. In other assays, 10 μg/ml of anti-CD3 and
881 5 μg/ml of the secondary antibody were used to cross-link the TCRs and thereby induce
882 store depletion. ~5 minutes post-store-depletion, Calcium Chloride ($CaCl_2$) was added
883 back to the dish at a final concentration of 2 mM to estimate the magnitude of store
884 operated calcium entry.
885
886 **Degranulation assay**
887 PBMCs were cultured in RPMI containing 10% FBS and 50 ng/ml IL-2 and stimulated
888 with PHA (2 μg /ml) 48hrs before the assay. 24hrs prior to the assay, IL-2 was washed
889 off but PHA was re-added. On the day of the assay cells were washed twice to remove
890 PHA and any growth factors. To measure degranulation, cells were either left
891 unstimulated, stimulated with a combination of anti-CD3 (10 μg/ml plate-coated), anti-
892 CD28 (2 μg/ml soluble) and anti-CD49d (2 μg/ml soluble) or a combination of Ionomycin
893 (1 μM) and PMA (50 ng/ml) for 3.5 hours. CD107a-PE antibody (1:50 dilution) was added
894 to each of the three groups at the start of stimulation. Following stimulations, cells were
895 transferred to ice, washed with cold HBSS containing 2% FBS and incubated with anti-
896 CD8 APC for 20 minutes, washed twice with cold HBSS and analyzed using Cytoflex
897 (Beckman Coulter) flow cytometer.
898
899 **qPCR to estimate gene expression in human PBMCs**
900 PBMCs were taken off IL-2 48 hours prior to the assay. On the day of the assay, cells
901 were washed twice, left unstimulated and either stimulated with anti-CD3 (10 μg/ml, plate-
902 coated), anti-CD28 (2 μg/ml) and anti-CD49d (2 μg/ml) or with Ionomycin (1 μM) and PMA
903 (50 ng/ml) for 6 hours. To end the stimulation, cells were washed with cold HBSS, pelleted
904 and used for RNA extraction. Total RNA was isolated using Qiagen RNeasy mini kit and
905 cDNA was synthesized using random hexamers and Superscript IV (Invitrogen). cDNA
906 was quantified using Qubit and subjected to QPCR analysis using Taqman probes for IL-

907 2 and beta-actin housekeeping gene control in triplicates. Analysis was performed by
908 calculating the double delta C_t values.
909
910 **Transduction of human PBMCs with pMSCV-STX11**
911 For viral transduction of PBMCs, polystyrene non-TC treated 24-well plates were coated
912 with retronection (20 μg/ml) overnight at 4°C, blocked with 2% BSA for 30 minutes at
913 room temperature and washed twice with HBSS. The retroviral supernatants were added
914 onto the coated wells and the plates were spun at 1800g for 2 hours at 30°C. Following
915 spin, the wells were washed with the blocking solution. PBMCs cultured in RPMI
916 containing 10% FBS were stimulated with PHA (2 μg/ml) and IL-2 (50 ng/ml) for 48 hours
917 prior to transduction. Stimulated PBMCs were transferred to coated plates at a density of
918 0.25 million cells/well centrifuged at 400g for 40 minutes at 30°C. The cells were analyzed
919 48-72 hours post transduction.
920
921 **Patch clamp measurements**
922 Patch clamp recordings were performed by using an Axopatch 200B amplifier (Axon
923 Instruments, Foster City, CA) interfaced to an ITC-18 input/output board (Instrutech, Port
924 Washington, NY) and an iMac G5 computer. Currents were filtered at 1 kHz with a four-
925 pole Bessel filter and sampled at 5 kHz. Recording electrodes were pulled from 100-μl
926 pipettes (VWR), coated with Sylgard, and fire-polished to a final resistance of 2 to 5 MΩ.
927 Stimulation and data acquisition and analysis were performed by using in-house routines
928 developed by RS Lewis (Stanford University) on the Igor Pro platform (Wavemetrics, Lake
929 Oswego, OR). All data were corrected for the liquid junction potential of the pipette
930 solution relative to Ringer's in the bath (-10 mV) and for leak currents collected in 20 mM
931 extracellular free calcium plus 10μM La^{3+}. The holding potential was +30 mV. The
932 standard voltage stimulus consisted of a 100-ms step to –100 mV followed by a 100-ms
933 ramp from –100 to +100 mV applied at 1 s intervals. I_{CRAC} was typically activated by
934 passive depletion of ER Ca^{2+} stores by intracellular dialysis of 8 mM BAPTA.
935
936 **Solutions and chemicals**

937 The standard extracellular Ringer solution contained 130 mM NaCl, 4.5 mM KCl, 20 mM
938 $CaCl_2$, 10 mM tetraethylammoniumchloride (TEA-Cl), 10 mM D -glucose and 5 mM
939 HEPES (pH 7.4 with NaOH). The standard divalent-free (DVF) Ringer solutions contained
940 (in mM) 150 NaCl, 10 HEDTA, 1 EDTA, and 10 HEPES (pH 7.4). The internal solution
941 contained: 135 mM Cs aspartate, 8 mM $MgCl_2$, 8 mM Cs-BAPTA and 10 mM HEPES (pH
942 7.2 with CsOH).
943
944 **Data analysis**
945 Analysis of current amplitudes was typically performed by measuring the peak currents
946 during the -100 mV pulse. Averaged results are presented as the mean value standard
947 error of the mean (SEM). Reversal potentials were measured from the average of several
948 leak-subtracted sweeps (4–6) in each cell. For datasets with two groups, statistical
949 analysis was performed with two- tailed t test to compare between control and test
950 conditions with a confidence level of 95%, and results with $p<0.05$ were considered
951 statistically significant.
952
953 **STX11:Orai1 and SOAR:Orai complex prediction**
954 Full length STX11 and its two domains, (H_{abc} 41-167 and SNARE 183-267) and Orai1 (N-
955 terminus 1-87 and C-terminus 256-301) were used to generate the complex of STX11
956 and Orai1 using AlphaFold3 (AF3) in all combinations. For Stim1, SOAR, residue 344-
957 444 were used along with Orai C-terminus 256-301. The resultant models were assessed
958 using ipTM and pTM scores. The best scoring combinations were further considered to
959 generate more models by changing the seed values. The best model in terms of highest
960 ipTM and pTM values was considered for further analysis. Custom script was used to
961 analyze the contact frequency of interacting residues of STX11-H_{abc} and Orai1 C-terminus
962 complex as well as SOAR and Orai1 C-terminus, across all predicted models.
963
964 **Molecular dynamics (MD) simulation**
965 The STX11 H_{abc}:Orai1 C-terminus and SOAR:Orai1 C-terminus complexes were
966 subjected to all-atom MD simulations. Initially, the complexes were prepared using
967 protein-preparation module of Schrodinger which involves H-bond network optimization

968 and restrained minimization of the initial structure. The prepared structures were solvated
969 using TIP3P water model in an orthorhombic box and neutralized by adding counter ions.
970 OPLS4 force field was used, and simulation system was generated by specifying 150 mM
971 salt (NaCl). The solvated system was subjected to default relaxation protocol of Desmond
972 followed by production run for 500 ns at 300K and 1 atm pressure in NPT ensemble. The
973 default relaxation protocol includes several short simulation steps. (1) Brownian dynamics
974 simulation for 100 ps at 10 K temperature in NVT with restraints on solute heavy atoms
975 (2) Simulation in NVT ensemble at 10 K for 12 ps with restraints on solute heavy atoms
976 (3) 12 ps simulation in NPT ensemble at 10 K with restraints on solute heavy atoms (4)
977 Simulation in NPT ensemble for 12 ps with restraints on solute heavy atoms (5) Simulation
978 in NPT ensemble for 24 ps without restraints. Three independent runs were executed with
979 different initial seeds for both structures.
980
981 **Analysis of MD simulation**
982 The MD runs were analyzed for the stability of the complex and interactions between the
983 subunits. The RMSD was calculated using simulation interaction diagram (SID) module
984 of Schrodinger. The first frame was used as reference frame for RMSD calculation. Script
985 "analyze_trajectory_ppi.py" was used to calculate the interactions between STX11:Orai1
986 and Stim1:Orai1. The binding energy (ΔG) at each nanosecond across simulation was
987 calculated using "thermal_mmgbsa.py" script of Schrodinger. The representative
988 structure was generated through trajectory clustering. The last 200 ns frames from each
989 run were combined and clustered using scripts "trj_merge.py" and "trajectory cluster" of
990 Schrodinger. The cluster representative of the largest cluster was used to analyze the
991 protein-protein interactions. PDB Sum was used to calculate the interactions in the cluster
992 representative. Figures were generated using Pymol and MD movies using Maestro.
993
994 **Statistical Analysis**
995 Statistical analysis was done using unpaired two-tailed Student's *t* test where only two
996 groups were being compared and ANOVA where more than two groups were present.
997 Normality of distribution was checked in Origin. Mann Whitney U Test was used for

datasets with non-normal (or skewed) distribution. P values for all significance tests were *P<0.05; **P<0.01; ***P<0.001.

Acknowledgements: We thank Vivien Beziat, Yenan Bryceson, Heinrich Schlums, Jelve Nejati Zendegani, Stephan Ehl, and Jasmin Mann for help with human PBMC handling, isolation, storage and shipping. Anand Vaidya for advice on STX11 purification. Jyoti Rohilla for technical support. Bio Render for the generation of models and IBS 2.0 for the generation of schematics shown in this manuscript. This work was supported in part by Department of Atomic Energy, Government of India under Project Identification No. RTI 4007 and NIH-NIAID grant AI108636.

1029 **References:**

1030

1031 1. Zhang, K., et al., *Familial Hemophagocytic Lymphohistiocytosis*, in *GeneReviews((R))*,
1032 M.P. Adam, et al., Editors. 1993: Seattle (WA).
1033 2. D'Orlando, O., et al., *Syntaxin 11 is required for NK and CD8(+) T-cell cytotoxicity and*
1034 *neutrophil degranulation.* Eur J Immunol, 2013. **43**(1): p. 194-208.
1035 3. Clapham, D.E., *Calcium signaling.* Cell, 2007. **131**(6): p. 1047-58.
1036 4. Vig, M. and J.P. Kinet, *The long and arduous road to CRAC.* Cell Calcium, 2007. **42**(2): p.
1037 157-62.
1038 5. Vig, M., et al., *Defective mast cell effector functions in mice lacking the CRACM1 pore*
1039 *subunit of store-operated calcium release-activated calcium channels.* Nat Immunol,
1040 2008. **9**(1): p. 89-96.
1041 6. Maul-Pavicic, A., et al., *ORAI1-mediated calcium influx is required for human cytotoxic*
1042 *lymphocyte degranulation and target cell lysis.* Proc Natl Acad Sci U S A, 2011. **108**(8): p.
1043 3324-9.
1044 7. Vig, M., et al., *CRACM1 multimers form the ion-selective pore of the CRAC channel.* Curr
1045 Biol, 2006. **16**(20): p. 2073-9.
1046 8. Vig, M., et al., *CRACM1 is a plasma membrane protein essential for store-operated Ca2+*
1047 *entry.* Science, 2006. **312**(5777): p. 1220-3.
1048 9. Miao, Y., et al., *An essential and NSF independent role for alpha-SNAP in store-operated*
1049 *calcium entry.* Elife, 2013. **2**: p. e00802.
1050 10. Prakriya, M. and R.S. Lewis, *Store-Operated Calcium Channels.* Physiol Rev, 2015. **95**(4):
1051 p. 1383-436.
1052 11. Feske, S., et al., *A mutation in Orai1 causes immune deficiency by abrogating CRAC*
1053 *channel function.* Nature, 2006. **441**(7090): p. 179-85.
1054 12. Zhang, S.L., et al., *Genome-wide RNAi screen of Ca(2+) influx identifies genes that*
1055 *regulate Ca(2+) release-activated Ca(2+) channel activity.* Proc Natl Acad Sci U S A, 2006.
1056 **103**(24): p. 9357-62.
1057 13. Yoon, T.Y. and M. Munson, *SNARE complex assembly and disassembly.* Curr Biol, 2018.
1058 **28**(8): p. R397-R401.
1059 14. Li, P., et al., *alpha-SNAP regulates dynamic, on-site assembly and calcium selectivity of*
1060 *Orai1 channels.* Mol Biol Cell, 2016. **27**(16): p. 2542-53.
1061 15. Miao, Y., et al., *Na+ influx via Orai1 inhibits intracellular ATP induced mTORC2 signaling*
1062 *to disrupt CD4 T cell gene expression and differentiation.* Elife, 2017. **6**.
1063 16. Ramanagoudr-Bhojappa, R., Y. Miao, and M. Vig, *High affinity associations with alpha-*
1064 *SNAP enable calcium entry via Orai1 channels.* PLoS One, 2021. **16**(10): p. e0258670.
1065 17. Jarvis, S.E. and G.W. Zamponi, *Masters or slaves? Vesicle release machinery and the*
1066 *regulation of presynaptic calcium channels.* Cell Calcium, 2005. **37**(5): p. 483-8.
1067 18. Vig, M. and J.P. Kinet, *Calcium signaling in immune cells.* Nature immunology, 2009.
1068 **10**(1): p. 21-7.
1069 19. Bryceson, Y.T., et al., *Defective cytotoxic lymphocyte degranulation in syntaxin-11*
1070 *deficient familial hemophagocytic lymphohistiocytosis 4 (FHL4) patients.* Blood, 2007.
1071 **110**(6): p. 1906-15.

1072 20. Hackmann, Y., et al., *Syntaxin binding mechanism and disease-causing mutations in*
1073 *Munc18-2.* Proc Natl Acad Sci U S A, 2013. **110**(47): p. E4482-91.
1074 21. Hellewell, A.L., et al., *Analysis of familial hemophagocytic lymphohistiocytosis type 4*
1075 *(FHL-4) mutant proteins reveals that S-acylation is required for the function of syntaxin*
1076 *11 in natural killer cells.* PLoS One, 2014. **9**(6): p. e98900.
1077 22. Jahn, R. and R.H. Scheller, *SNAREs--engines for membrane fusion.* Nat Rev Mol Cell Biol,
1078 2006. **7**(9): p. 631-43.
1079 23. Li, Z., et al., *Graded activation of CRAC channel by binding of different numbers of STIM1*
1080 *to Orai1 subunits.* Cell Res, 2011. **21**(2): p. 305-15.
1081 24. McNally, B.A., et al., *Gated regulation of CRAC channel ion selectivity by STIM1.* Nature,
1082 2012. **482**(7384): p. 241-5.
1083 25. Peinelt, C., et al., *Amplification of CRAC current by STIM1 and CRACM1 (Orai1).* Nat Cell
1084 Biol, 2006. **8**(7): p. 771-3.
1085 26. Mercer, J.C., et al., *Large store-operated calcium selective currents due to co-expression*
1086 *of Orai1 or Orai2 with the intracellular calcium sensor, Stim1.* J Biol Chem, 2006.
1087 **281**(34): p. 24979-90.
1088 27. Soboloff, J., et al., *Orai1 and STIM reconstitute store-operated calcium channel function.*
1089 J Biol Chem, 2006. **281**(30): p. 20661-20665.
1090 28. Hou, X., S.R. Burstein, and S.B. Long, *Structures reveal opening of the store-operated*
1091 *calcium channel Orai.* Elife, 2018. **7**.
1092 29. Zhou, Y., et al., *The STIM1-binding site nexus remotely controls Orai1 channel gating.*
1093 Nat Commun, 2016. **7**: p. 13725.
1094 30. Cormet-Boyaka, E., et al., *CFTR chloride channels are regulated by a SNAP-23/syntaxin*
1095 *1A complex.* Proc Natl Acad Sci U S A, 2002. **99**(19): p. 12477-82.
1096 31. Toft-Bertelsen, T.L., et al., *Regulation of Ca2+ channels by SNAP-25 via recruitment of*
1097 *syntaxin-1 from plasma membrane clusters.* Mol Biol Cell, 2016. **27**(21): p. 3329-3341.
1098 32. Jessen, B., et al., *Graded defects in cytotoxicity determine severity of hemophagocytic*
1099 *lymphohistiocytosis in humans and mice.* Front Immunol, 2013. **4**: p. 448.
1100 33. Chinn, I.K., et al., *Genetic and mechanistic diversity in pediatric hemophagocytic*
1101 *lymphohistiocytosis.* Blood, 2018. **132**(1): p. 89-100.
1102 34. Dulubova, I., et al., *Munc18-1 binds directly to the neuronal SNARE complex.* Proc Natl
1103 Acad Sci U S A, 2007. **104**(8): p. 2697-702.
1104 35. Lee, S., et al., *Munc18-1 induces conformational changes of syntaxin-1 in multiple*
1105 *intermediates for SNARE assembly.* Sci Rep, 2020. **10**(1): p. 11623.
1106 36. Park, C.Y., et al., *STIM1 clusters and activates CRAC channels via direct binding of a*
1107 *cytosolic domain to Orai1.* Cell, 2009. **136**(5): p. 876-90.
1108 37. Stathopulos, P.B., et al., *STIM1/Orai1 coiled-coil interplay in the regulation of store-*
1109 *operated calcium entry.* Nat Commun, 2013. **4**: p. 2963.
1110 38. Delevoye, C., et al., *Conservation of the biochemical properties of IncA from Chlamydia*
1111 *trachomatis and Chlamydia caviae: oligomerization of IncA mediates interaction*
1112 *between facing membranes.* J Biol Chem, 2004. **279**(45): p. 46896-906.
1113 39. Paumet, F., et al., *Intracellular bacteria encode inhibitory SNARE-like proteins.* PLoS One,
1114 2009. **4**(10): p. e7375.

40. Barocchi, M.A., V. Masignani, and R. Rappuoli, *Opinion: Cell entry machines: a common theme in nature?* Nat Rev Microbiol, 2005. **3**(4): p. 349-58.
41. Neveu, E., et al., *Prototypic SNARE Proteins Are Encoded in the Genomes of Heimdallarchaeota, Potentially Bridging the Gap between the Prokaryotes and Eukaryotes.* Curr Biol, 2020. **30**(13): p. 2468-2480 e5.

1148 **Figure Legends:**

1149

1150 **Figure 1: STX11 is required for SOCE.** Measurement of SOCE in STX11 depleted
1151 Jurkat and FHLH4 patient T cells. (**A-B**) Representative Fura-2 calcium imaging assay
1152 (**A**) and quantification of independent repeats (**B**) measuring thapsigargin (TG) induced
1153 SOCE in Jurkat T cells treated with scr (black), STX11#1 (red) or STX11#2 (blue)
1154 shRNAs. (n=30-40 cells/group, N=3). (**C-D**) Representative Fura-2 calcium imaging
1155 assay (**C**) and quantification of repeats (**D**) showing reconstitution of SOCE in STX11
1156 depleted Jurkat T cells by ectopic expression of STX11. scr shRNA with empty vector
1157 (EV) expression (black), STX11 shRNA with EV expression (red), STX11 shRNA with
1158 STX11 expression (green). (**E**) Sanger sequencing of FHLH4 patient DNA showing
1159 deletion of a single Adenine at the 752nd position and the resulting frameshift. (**F**)
1160 Schematic showing the predicted domain distribution of the wildtype *versus* FHLH4
1161 mutant STX11 protein. (**G**) Western blot on WCLs of healthy donor (HD) and FHLH4
1162 patient PBMCs showing the relative molecular weight and abundance of the wildtype and
1163 mutant STX11 bands. (**H**) Western blot on WCLs of HEK293 cells over-expressing
1164 wildtype or FHLH4 mutant STX11 and empty vector. (**I**) Fura-2 calcium imaging assay
1165 measuring anti-CD3 induced SOCE in HD (black) and FHLH4 (red) T cells. (n=30-40
1166 cells/group). (**J**) Fura-2 calcium imaging assay measuring SOCE in HD expressing empty
1167 vector (EV) (black) and FHLH4 T cells expressing human STX11 (red), respectively.
1168 (n=30-40 cells/group). (**K-L**) Representative Fura-2 calcium imaging assay (**K**) and
1169 quantification of repeats (**L**) measuring SOCE in Jurkat T cells treated either with scr
1170 shRNA expressing empty vector (EV) (black), STX11 shRNA, expressing EV (red),
1171 STX11 shRNA, expressing wildtype STX11 (green), STX11 shRNA, expressing FHLH4
1172 mutant STX11 (blue).

1173 **Figure 2. STX11 regulates I_{CRAC}.** (**A-D**) Measurement of I_{CRAC} in STX11 depleted Jurkat
1174 T-cells in the whole-cell recording configuration in 20 mM extracellular Ca^{2+} Ringer's
1175 solution. I_{CRAC} was induced by passive depletion of intracellular Ca^{2+} stores by dialyzing
1176 8 mM BAPTA into the cell via the patch-pipette. (**A**) Representative current at -100 mV
1177 in Jurkat T cells treated with scr shRNA construct. The current is blocked by extracellular

1178 La^{3+} (10 μM) and replacing the 20 mM Ca^{2+} Ringer's solution with a divalent free solution
1179 (DVF) evokes a large Na^{+} current which depotentiates over tens of seconds. The current-
1180 voltage (I-V) relationship of the Ca^{2+} and DVF currents are shown on the
1181 right. (**B**) I_{CRAC} from a Jurkat T cell treated with STX11 shRNA. Both Ca^{2+} and Na^{+} current
1182 amplitudes are reduced relative to control cells. The I-V relationships (*right plots)* show
1183 no change in ion selectivity. (**C-D**) Summary of the current amplitudes of Ca^{2+} and
1184 Na^{+} currents and current reversal potentials in scr and STX11 knockdown cells.

1185 **Figure 3. STX11 regulates NFAT activation, IL-2 gene expression and degranulation**
1186 **in FHLH4 patient T cells.** (**A-C**) Estimation of nuclear translocation of NFAT. (**A**) Western
1187 blot showing nuclear translocation of NFAT in Jurkat T cells treated with scr or STX11
1188 shRNA and stimulated with PMA+TG. N=3. (**B**) Representative confocal images of control
1189 and STX11 depleted Jurkat T cells stimulated with anti-CD3, immunolabelled with anti-
1190 NFAT1 antibody and counter-stained with DAPI. (N=3) (**C**) Box and whisker plot showing
1191 quantification of nuclear NFAT from cells populating 10 randomly chosen fields per group
1192 in (**B**). (**D**) Quantification of IL-2 mRNA in anti-CD3 stimulated Jurkat T cells treated with
1193 scr or STX11 shRNA using qPCR. The bars show mean ± SE of relative IL-2 mRNA. N=3.
1194 (E) Quantification of IL-2 EIA on supernatants of scr (black) or STX11 (red) shRNA treated
1195 Jurkat T cells stimulated with anti-CD3. (**F**) qPCR analysis of IL-2 mRNA expression in
1196 various stimulated HD (black) and FHLH4 T cells (red). (**G-H**) Granule release assay
1197 performed on HD (black) and FHLH4 CD8 T (red) cells (**G**) and its quantification (**H**).
1198

1199 **Figure 4: STX11 directly binds resting Orai1 in plasma membrane.** Intracellular
1200 localization of STX11 and its association with Orai1. (**A**) Representative confocal images
1201 of HEK293 cells transfected with either HA-tagged STX11 or untagged STX11 and
1202 stained using anti-HA antibody or anti-STX11 antibody respectively. N=3 (**B**) Localization
1203 of HA-tagged STX11 with respect to Orai1-YFP in the basal as well as nuclear plane of
1204 HEK293 cells. N=3 (**C-D**) Co-IP to assess STX11 binding to Orai1. Whole cell lysates of
1205 resting and store-depleted HEK293 cells co-expressing either Flag-Orai1 and STX11 (**C**)
1206 or Orai1-Myc and STX11 (**D**) were subjected to IP and Western blot using anti-Myc, anti-
1207 Flag or anti-STX11 antibodies, as indicated. (N=3) **(E)** Schematic showing key domains

1208 of STX11 and Orai1 used for *in vitro* pull-down assays. (**F**) Pull-down assay showing *in*
1209 *vitro* binding of His-tagged STX11 to Orai1. (Top) Ponceau S staining showing the input
1210 of MBP alone or MBP-tagged Orai1 fragments. (Bottom) Western blot using anti-STX11
1211 antibody. Input:1/5th of the protein. N=4. (**G**) Pull-down assay showing *in vitro* binding of
1212 His-tagged H_{abc} domain of STX11 to Orai1 fragments. (Top) Ponceau S staining showing
1213 the input of MBP alone or MBP-tagged Orai1 fragments. Input:1/5th of the protein.
1214 (Bottom) Western blot using anti-His antibody. N=3. (**H**) Binding free energy distribution
1215 of STX11-H_{abc} and Orai1 C-terminus interactions. (**I**) Sphere and cartoon representation
1216 of the structure of STX11 H_{abc} (green) and Orai1 C-terminus (cyan) complex after MD
1217 simulation. The N-termini are highlighted in blue, and C-termini in red. (**J**) Representative
1218 confocal images showing localization of STX11 with respect to Orai1:Stim1 puncta in
1219 store-depleted cells. HEK293 cells expressing Orai1-YFP, CFP-Stim1 were transfected
1220 with HA-tagged STX11, store-depleted and stained using anti-HA antibody. (N=3) (**K**)
1221 Quantification of the localization of STX11 with respect to Stim1:Orai1 puncta in store-
1222 depleted cells.
1223
1224 **Figure 5. Residues involved in Orai1:STX11 complex formation are crucial for**
1225 **SOCE.** Analysis of STX11 and Orai1 mutants. (**A**) Schematic showing STX11 mutations
1226 (Top). Expression of wildtype STX11 or STX11 N147A_E150A mutant in HEK293
1227 followed by immunolabeling (**A**, bottom) and Western blot (**B**) using anti-STX11 antibody.
1228 (**C-D**) Representative Fura-2 calcium imaging assay (**C**) and quantification of repeats (**D**)
1229 measuring rescue of SOCE in Jurkat cells treated either with scr shRNA (black) or STX11
1230 shRNA expressing empty vector (red), wildtype STX11 (green) or N147A_E150A mutant
1231 STX11 (blue). (**E**) Coomassie blue stained SDS-PAGE showing expression and
1232 purification of His-tagged wildtype or N147A_E150A mutant STX11 from *E. coli.* (**F**) Pull-
1233 down assay measuring their binding to MBP-tagged Orai1 C-terminus. (Top) Ponceau S
1234 staining showing the input of MBP-tagged fragments. (Bottom) Western blot using anti-
1235 STX11 antibody. N=4 (**G**) Schematic showing Orai1 mutations (Top). Confocal images of
1236 HEK293 cells expressing YFP-tagged wildtype or R289A_E272A_E275A_E278A mutant
1237 Orai1 (Bottom). **(H-I)** Representative Fura-2 calcium imaging assay (**H**) and quantification
1238 of repeats (**I**) measuring rescue of SOCE in HEK293 cells treated either with scr (black)

1239 or Orai1 shRNA expressing empty vector (red), wildtype Orai1 (green) or
1240 R289A_E272A_E275A_E278A mutant Orai1 (blue). (**J**) Pull-down assay measuring the
1241 binding of MBP-tagged wildtype or R289A_E272A_E275A_E278A mutant Orai1 C-
1242 terminus to wildtype or N147A_E150A mutant STX11. (Top) Ponceau S staining showing
1243 the input of MBP-tagged Orai1 fragments. (Bottom) Western blot using anti-STX11
1244 antibody. N=4. (**K-L**) Representative confocal images (**K**) and quantification (**L**) of PM
1245 localized YFP-CAD in CFP-tagged wildtype or R289A_E272A_E275A_E278A mutant
1246 Orai1 expressing HEK293 cells.
1247
1248 **Figure 6: Orai1 clustering is dysfunctional in STX11 depleted cells.** Quantification of
1249 Orai1 and Stim1 intensities in the ER-PM puncta of store-depleted cells. (**A-B**)
1250 Representative confocal images of resting (**A**) and store-depleted (**B**) shRNA treated
1251 HEK293 cells expressing N-terminal CFP tagged Orai1 (CFP-Orai1) and C-terminal YFP
1252 tagged Stim1 (Stim1-YFP). (**C-F**) Mean Stim1-YFP intensity (**C**) and area (**D**) of Stim1
1253 clusters. Mean CFP-Orai1 intensities inside (**E**) and outside (**F**) Stim1-YFP clusters of
1254 shRNA treated cells, post store-depletion. (**G-J**) Quantification of Orai1 and Stim1
1255 intensities in the ER-PM puncta of C-terminal YFP-tagged Orai1 (Orai1-YFP) and N-
1256 terminal CFP-tagged Stim1 (CFP-Stim1). (**G-H**) Mean CFP-Stim1 intensity (**G**) and area
1257 (**H**) of Stim1 clusters. Mean Orai1-YFP intensity (**I**) and area (**J**) of Orai1-YFP clusters in
1258 control and STX11 depleted cells. (**K-L**) Representative Fura-2 calcium imaging assay
1259 (**K**) and quantification of repeats (**L**) measuring TG induced SOCE in Orai1-YFP and
1260 CFP-Stim1 expressing HEK293 cells treated with scr (black) or STX11 (red) shRNA.
1261
1262 **Figure 7: STX11 primes Orai1 for optimal on-site assembly.** Oligomerization of Orai1.
1263 **(A)** N-FRET analysis of scramble control and STX11 shRNA treated HEK293 cells co-
1264 expressing Orai1-CFP and Orai1-YFP before and after store-depletion. **(B&C)**
1265 Representative images (**B**) and quantification (**C**) of FRET analysis using acceptor
1266 photobleaching of control and STX11 shRNA treated Orai1 Stim1 double knockdown
1267 resting HEK293A cells co-expressing Orai1-CFP (donor) and Orai1-YFP (acceptor). **(D-**
1268 **E)** Representative western blot (**D**) and quantification of band intensities from repeats (**E**)
1269 showing distribution of BS3 crosslinked Flag-Orai1 oligomeric bands in control and

1270 STX11 depleted HEK293 cells. N=3. (**F-H**) Fura-2 calcium imaging assay (**F**) and
1271 quantification of repeats (**G-H**) to measure constitutive calcium influx in Orai1-CFP and
1272 YFP-CAD expressing, control (black) or STX11 depleted (red) HEK293 cells at 0 mM (**G**)
1273 and 2 mM (**H**) extracellular Ca^{2+}. (**I-J**) Fura-2 calcium imaging assay (**I**) and quantification
1274 of repeats (**J**) to measure constitutive calcium influx in Orai1-H134S mutant expressing
1275 control (black) and STX11 depleted (red) HEK293 cells. (**K-L**) Fura-2 calcium imaging
1276 assay (**K**) and quantification of repeats (**L**) to measure constitutive calcium influx in Orai1-
1277 ANSGA mutant expressing control (black) and STX11 depleted (red) HEK293 cells.
1278
1279 **Figure 8: Models depicting STX11 mediated priming of Orai1 and its role in T cell**
1280 **signaling and function.** (**A**) STX11 unbound (unprimed) and bound (primed) Orai1 in
1281 resting and store-depleted cells. For simplicity, STX11 interaction with only two subunits
1282 of Orai1 has been shown. (**B**) Regulation of T cell SOCE, NFAT activation and effector
1283 function by STX11.
1284
1285
1286 Due to BioRxiv file size limit, the Supplementary Movies can be found at the following
1287 link: https://www.dropbox.com/scl/fo/3j07d3sua4g58w3yfmyv7/AAKjvIiniA-
1288 z994hxV9DNHo?rlkey=e7yj5wyukvwg5seg1awkuctc4&st=z6vp57dr&dl=0
1289

1290 **Supplementary Movies 1-3: Molecular dynamic simulations of Orai1 C-terminus**
1291 **interaction with the STX11_H_{ABC} domain.**

1292 **Supplementary Movies 4-6: Molecular dynamic simulations of Orai1 C-terminus**
1293 **interaction with Stim1 SOAR domain.**
1294
1295

Figure 1

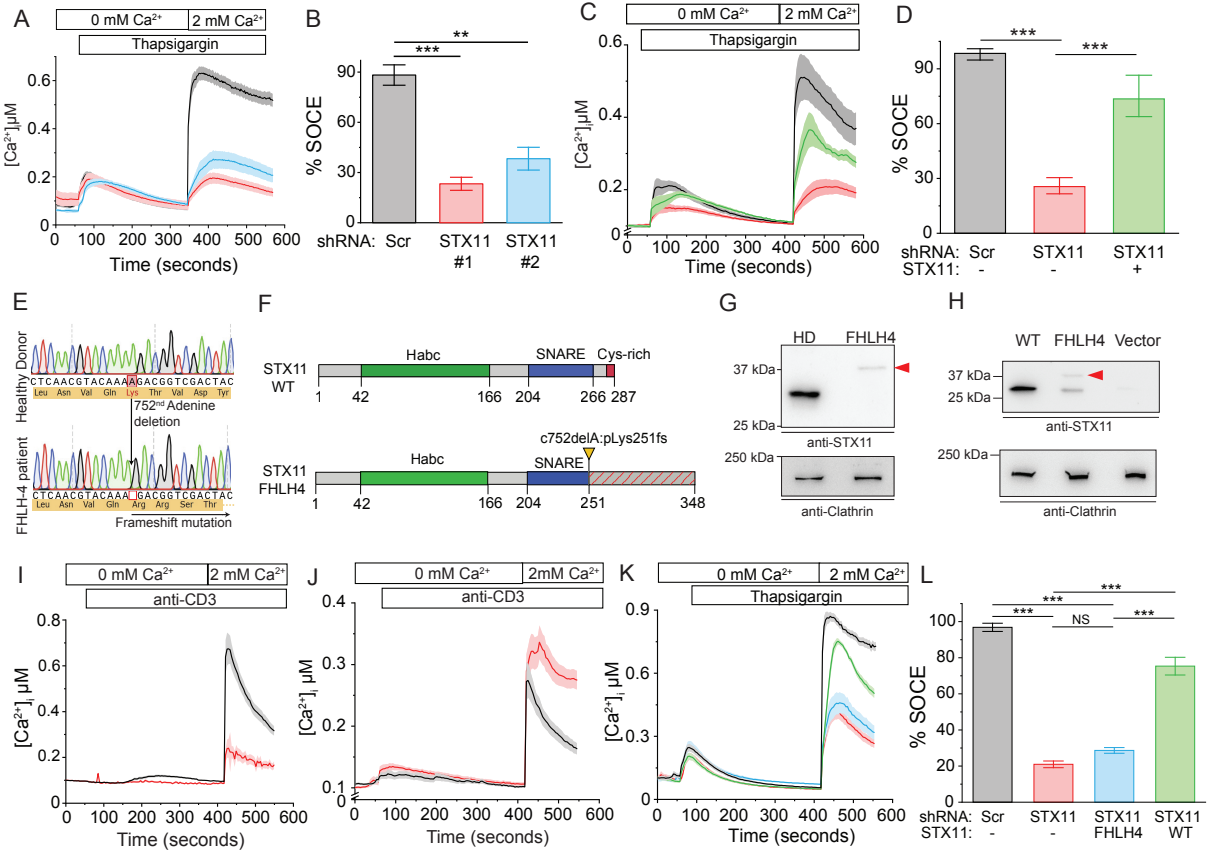
A
0 mM Ca2+
2 mM Ca2+
Thapsigargin
[Ca2+]µM
Time (seconds)
B
% SOCE
shRNA: Scr
STX11 #1
STX11 #2
C
0 mM Ca2+
2 mM Ca2+
Thapsigargin
[Ca2+]µM
Time (seconds)
D
% SOCE
shRNA: Scr
STX11: -
STX11 -
STX11 +
E
Healthy Donor
FHLH-4 patient
752nd Adenine deletion
Frameshift mutation
F
STX11 WT
Habc
SNARE
Cys-rich
STX11 FHLH4
c752delA:pLys251fs
G
HD
FHLH4
37 kDa
25 kDa
anti-STX11
250 kDa
anti-Clathrin
H
WT
FHLH4
Vector
37 kDa
25 kDa
anti-STX11
250 kDa
anti-Clathrin
I
0 mM Ca2+
2 mM Ca2+
anti-CD3
[Ca2+]i µM
Time (seconds)
J
0 mM Ca2+
2mM Ca2+
anti-CD3
[Ca2+]i µM
Time (seconds)
K
0 mM Ca2+
2 mM Ca2+
Thapsigargin
[Ca2+]i µM
Time (seconds)
L
% SOCE
NS
shRNA: Scr
STX11: -
STX11 -
STX11 FHLH4
STX11 WT

Figure 2

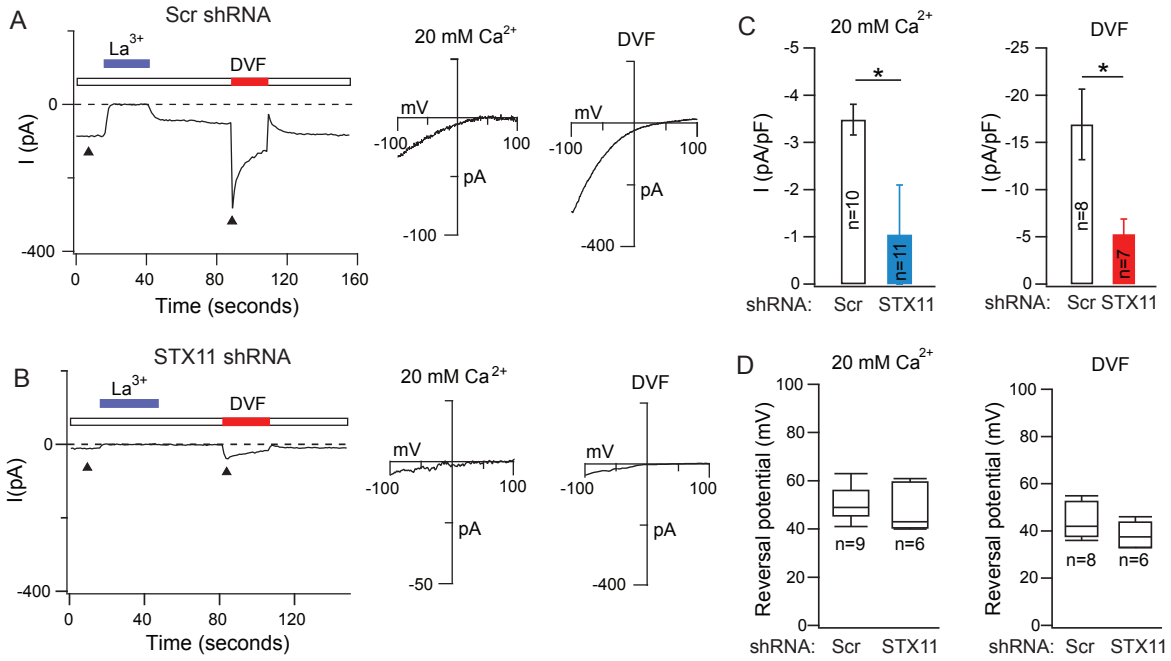
A
Scr shRNA
La3+
DVF
I (pA)
0
-400
0
40
80
120
160
Time (seconds)
20 mM Ca2+
mV
-100
100
pA
-100
DVF
mV
-100
100
pA
-400
C
20 mM Ca2+
I (pA/pF)
-5
-4
-3
-2
-1
0
*
n=10
n=11
shRNA: Scr STX11
DVF
I (pA/pF)
-25
-20
-15
-10
-5
0
*
n=8
n=7
shRNA: Scr STX11
B
STX11 shRNA
La3+
DVF
I(pA)
0
-400
0
40
80
120
Time (seconds)
20 mM Ca2+
mV
-100
100
pA
-50
DVF
mV
-100
100
pA
-400
D
20 mM Ca2+
Reversal potential (mV)
100
80
60
40
20
0
n=9
n=6
shRNA: Scr STX11
DVF
Reversal potential (mV)
100
80
60
40
20
0
n=8
n=6
shRNA: Scr STX11

Figure 3

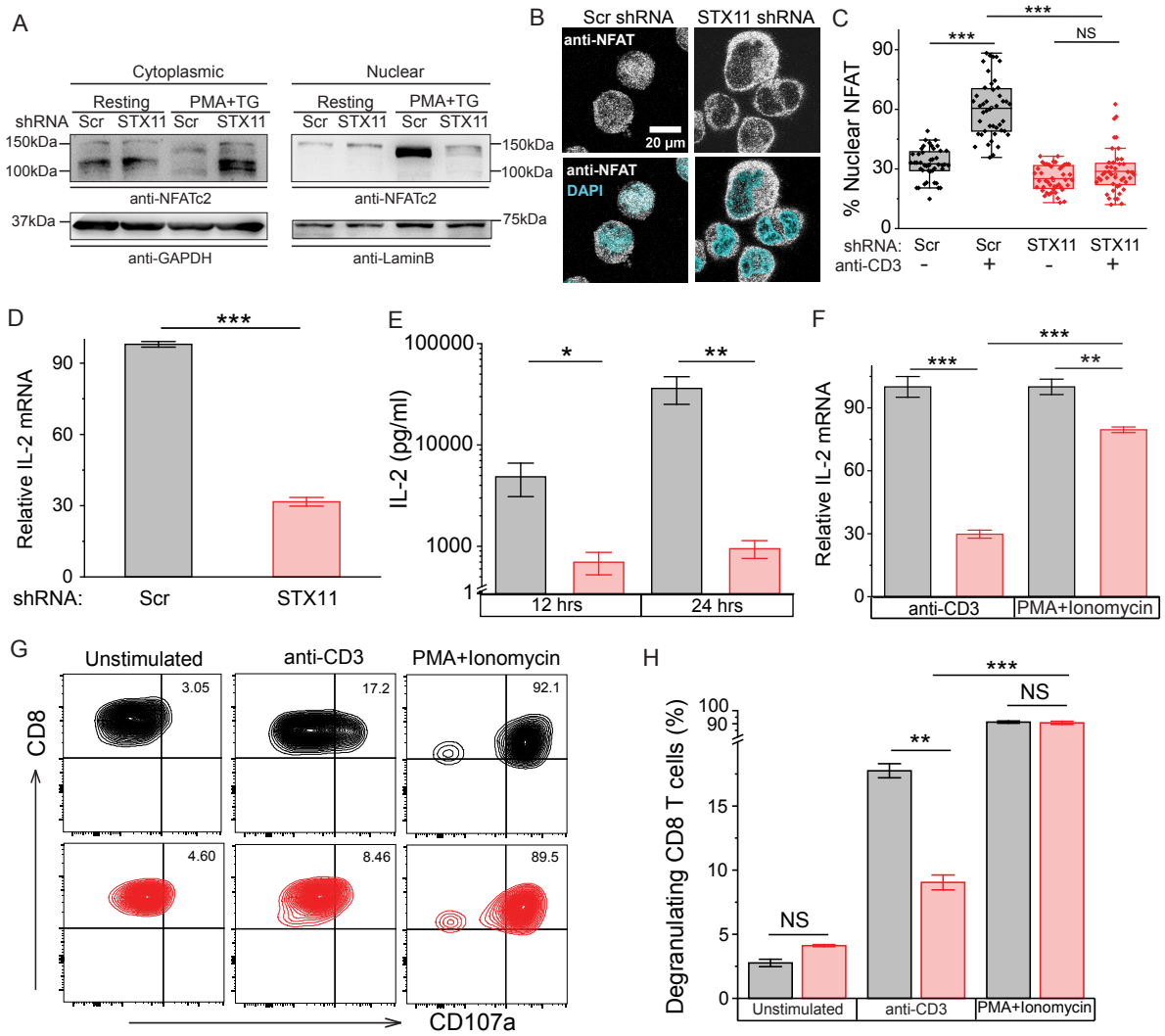
A
Cytoplasmic
Nuclear
Resting
PMA+TG
shRNA Scr STX11 Scr STX11
150kDa
100kDa
anti-NFATc2
37kDa
anti-GAPDH
75kDa
anti-LaminB
B
Scr shRNA
STX11 shRNA
anti-NFAT
20 µm
DAPI
C
% Nuclear NFAT
shRNA: Scr Scr STX11 STX11
anti-CD3 - + - +
NS
D
Relative IL-2 mRNA
shRNA: Scr STX11
E
IL-2 (pg/ml)
12 hrs
24 hrs
F
Relative IL-2 mRNA
anti-CD3
PMA+Ionomycin
G
Unstimulated
anti-CD3
PMA+Ionomycin
CD8
CD107a
3.05
17.2
92.1
4.60
8.46
89.5
H
Degranulating CD8 T cells (%)
Unstimulated
anti-CD3
PMA+Ionomycin
NS

Figure 4

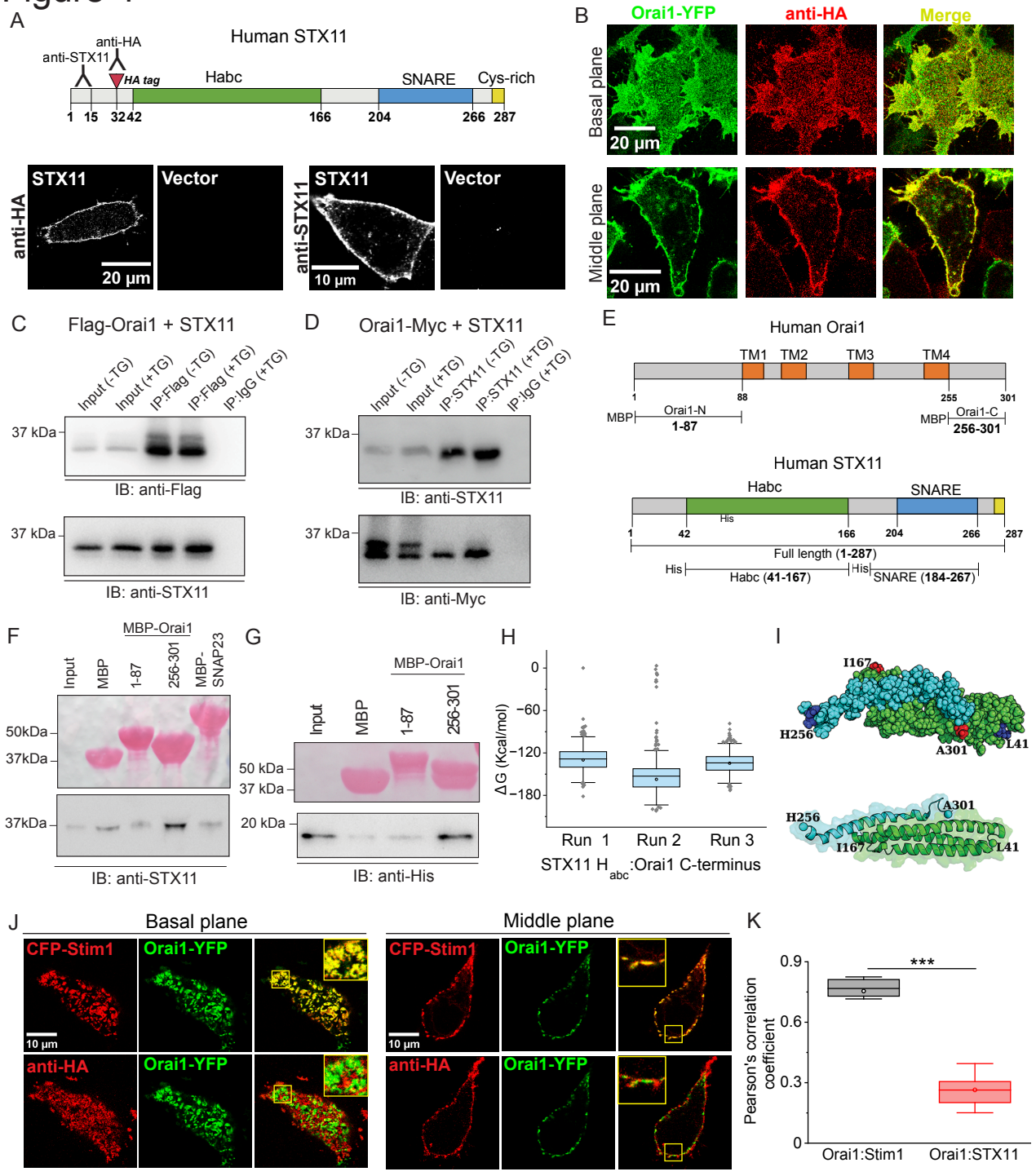
A
Human STX11
anti-HA
anti-STX11
HA tag
Habc
SNARE
Cys-rich
1 15 32 42 166 204 266 287
STX11
Vector
anti-HA
20 µm
STX11
Vector
anti-STX11
10 µm
B
Orai1-YFP
anti-HA
Merge
Basal plane
Middle plane
20 µm
20 µm
C
Flag-Orai1 + STX11
Input (-TG)
Input (+TG)
IP:Flag (-TG)
IP:Flag (+TG)
IP:IgG (+TG)
37 kDa
IB: anti-Flag
37 kDa
IB: anti-STX11
D
Orai1-Myc + STX11
Input (-TG)
Input (+TG)
IP:STX11 (-TG)
IP:STX11 (+TG)
IP:IgG (+TG)
37 kDa
IB: anti-STX11
37 kDa
IB: anti-Myc
E
Human Orai1
TM1 TM2 TM3 TM4
1 88 255 301
MBP
Orai1-N
1-87
MBP
Orai1-C
256-301
Human STX11
Habc
SNARE
His
1 42 166 204 266 287
Full length (1-287)
His
Habc (41-167)
His
SNARE (184-267)
F
MBP-Orai1
Input
MBP
1-87
256-301
MBP-SNAP23
50kDa
37kDa
37kDa
IB: anti-STX11
G
MBP-Orai1
Input
MBP
1-87
256-301
50 kDa
37 kDa
20 kDa
IB: anti-His
H
0
−60
−120
−180
ΔG (Kcal/mol)
Run 1
Run 2
Run 3
STX11 Habc:Orai1 C-terminus
I
I167
H256
A301
L41
H256
A301
I167
L41
J
Basal plane
Middle plane
CFP-Stim1
Orai1-YFP
10 µm
anti-HA
Orai1-YFP
CFP-Stim1
Orai1-YFP
10 µm
anti-HA
Orai1-YFP
K
0.9
0.6
0.3
0
***
Pearson's correlation coefficient
Orai1:Stim1
Orai1:STX11

Figure 5

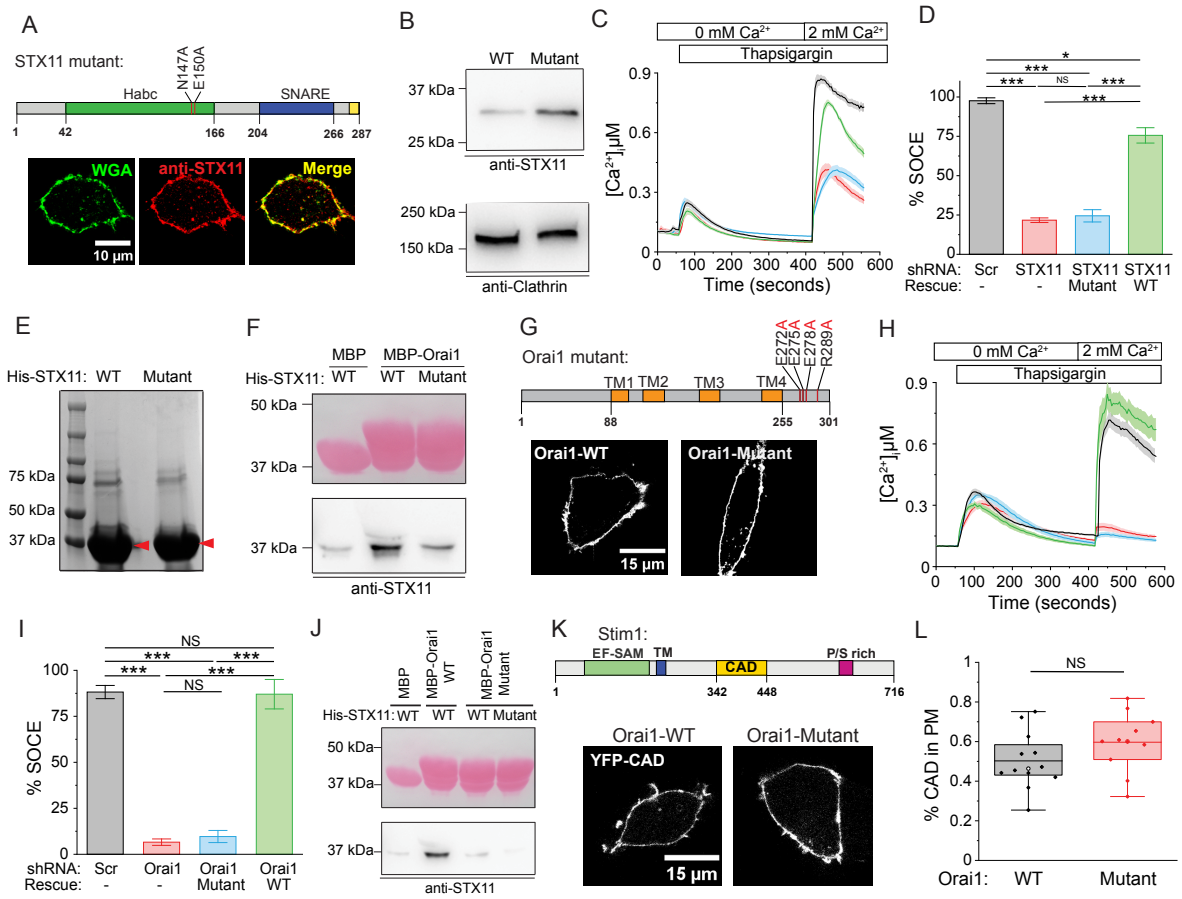
A
STX11 mutant:
N147A
E150A
Habc
SNARE
1
42
166
204
266
287
WGA
anti-STX11
Merge
10 µm
B
WT
Mutant
37 kDa
25 kDa
anti-STX11
250 kDa
150 kDa
anti-Clathrin
C
0 mM Ca2+
2 mM Ca2+
Thapsigargin
[Ca2+]µM
Time (seconds)
D
% SOCE
shRNA: Scr STX11 STX11 STX11
Rescue: - - Mutant WT
E
His-STX11: WT Mutant
75 kDa
50 kDa
37 kDa
F
MBP
MBP-Orai1
His-STX11: WT WT Mutant
50 kDa
37 kDa
anti-STX11
G
Orai1 mutant:
E272A
E275A
E278A
R289A
TM1 TM2 TM3 TM4
1
88
255
301
Orai1-WT
Orai1-Mutant
15 µm
H
0 mM Ca2+
2 mM Ca2+
Thapsigargin
[Ca2+]µM
Time (seconds)
I
% SOCE
shRNA: Scr Orai1 Orai1 Orai1
Rescue: - - Mutant WT
J
MBP
MBP-Orai1 WT
MBP-Orai1 Mutant
His-STX11: WT WT WT Mutant
50 kDa
37 kDa
anti-STX11
K
Stim1:
EF-SAM
TM
CAD
P/S rich
1
342
448
716
Orai1-WT
Orai1-Mutant
YFP-CAD
15 µm
L
% CAD in PM
Orai1: WT Mutant

Figure 6

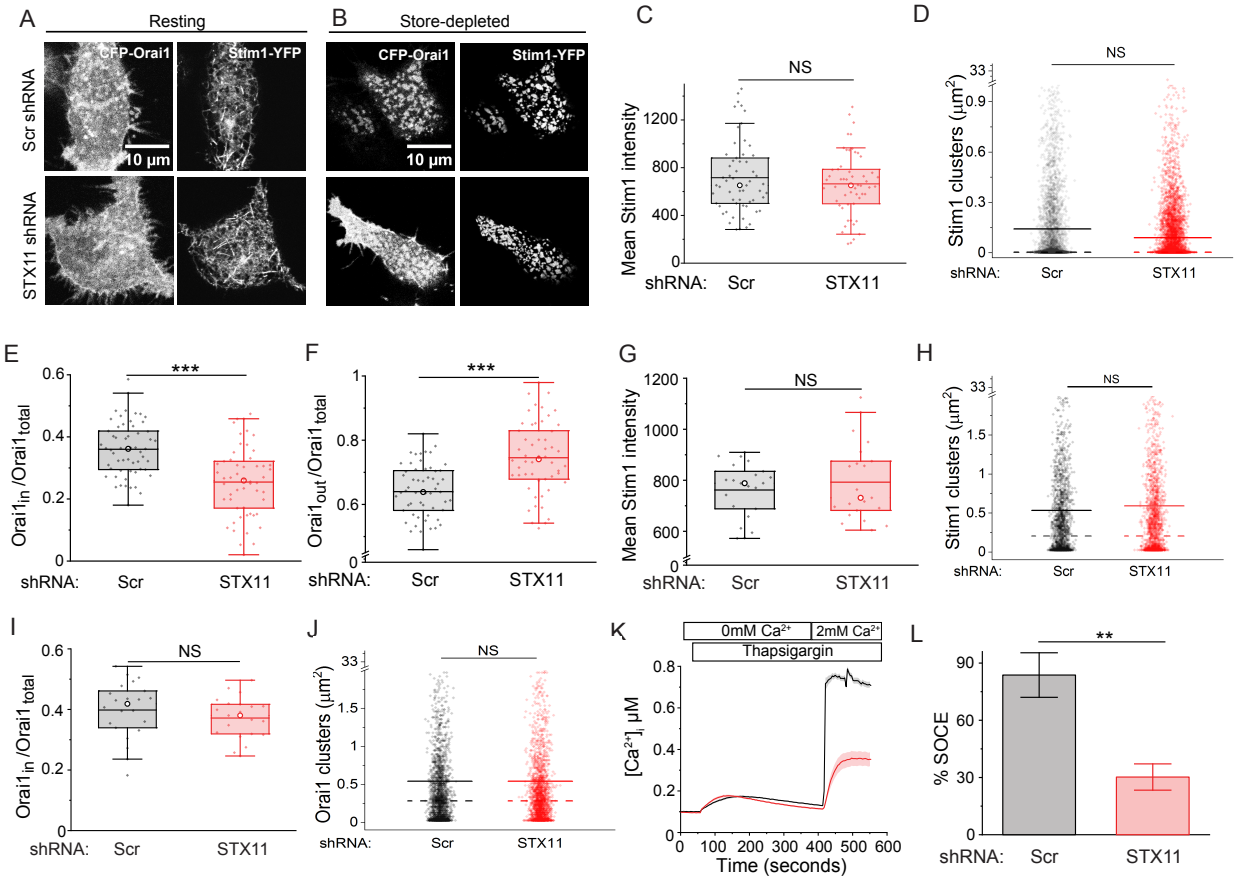
A
Resting
B
Store-depleted
CFP-Orai1
Stim1-YFP
Scr shRNA
STX11 shRNA
10 µm
C
Mean Stim1 intensity
NS
shRNA: Scr STX11
D
Stim1 clusters (µm²)
NS
E
Orai1in /Orai1total
***
F
Orai1out /Orai1total
***
G
Mean Stim1 intensity
NS
H
Stim1 clusters (µm²)
NS
I
Orai1in /Orai1total
NS
J
Orai1 clusters (µm²)
NS
K
0mM Ca2+
2mM Ca2+
Thapsigargin
[Ca2+]i µM
Time (seconds)
L
% SOCE
**

Figure 7

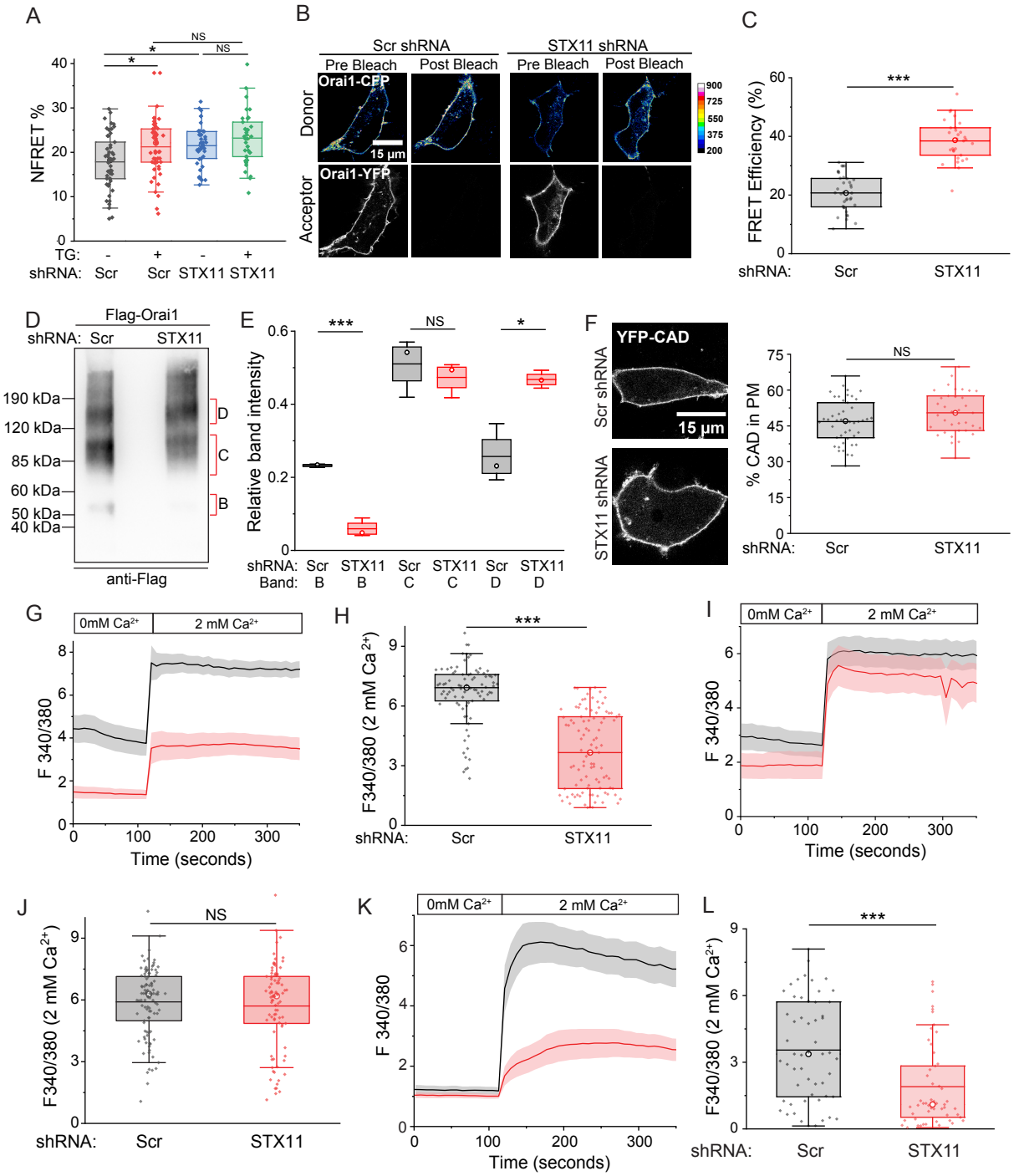
A
NFRET %
TG: - + - +
shRNA: Scr Scr STX11 STX11
NS
*
B
Scr shRNA
STX11 shRNA
Pre Bleach
Post Bleach
Donor
Acceptor
Orai1-CFP
Orai1-YFP
15 µm
900
725
550
375
200
C
FRET Efficiency (%)
***
shRNA: Scr STX11
D
Flag-Orai1
shRNA: Scr STX11
190 kDa
120 kDa
85 kDa
60 kDa
50 kDa
40 kDa
anti-Flag
E
Relative band intensity
***
NS
*
shRNA: Scr STX11 Scr STX11 Scr STX11
Band: B B C C D D
F
YFP-CAD
Scr shRNA
STX11 shRNA
15 µm
% CAD in PM
NS
shRNA: Scr STX11
G
0mM Ca2+
2 mM Ca2+
F 340/380
Time (seconds)
H
F340/380 (2 mM Ca2+)
***
shRNA: Scr STX11
I
0mM Ca2+
2 mM Ca2+
F 340/380
Time (seconds)
J
F340/380 (2 mM Ca2+)
NS
shRNA: Scr STX11
K
0mM Ca2+
2 mM Ca2+
F 340/380
Time (seconds)
L
F340/380 (2 mM Ca2+)
***
shRNA: Scr STX11

Figure 8

A **STX11 sufficient:**

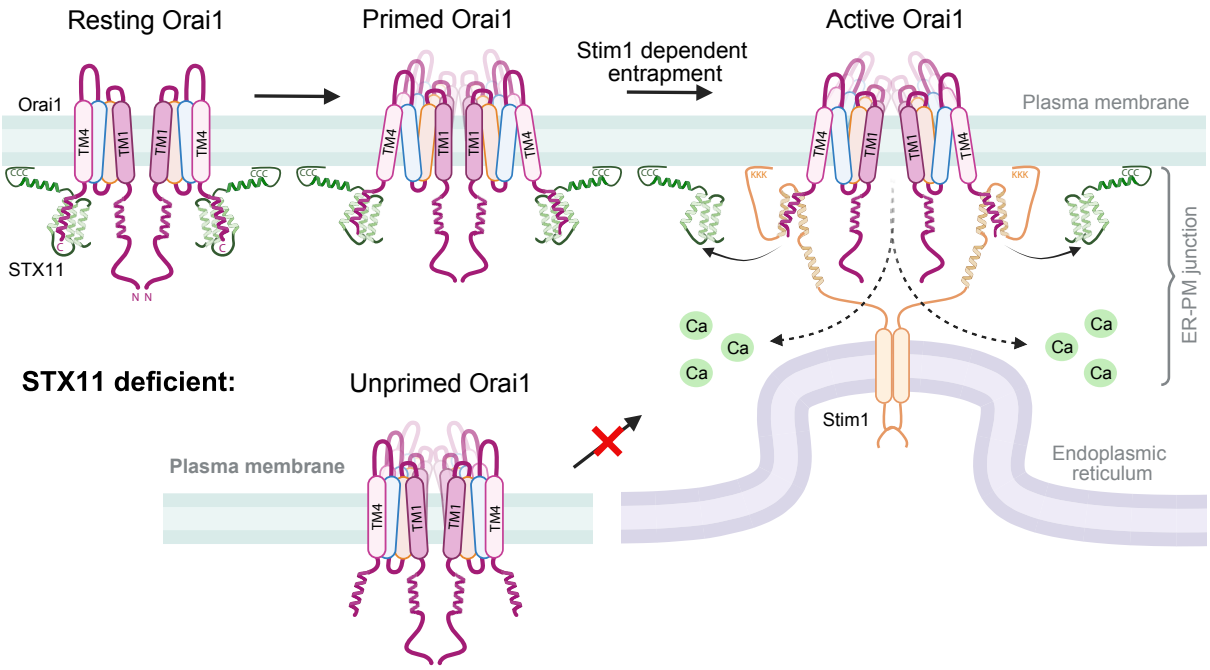

B

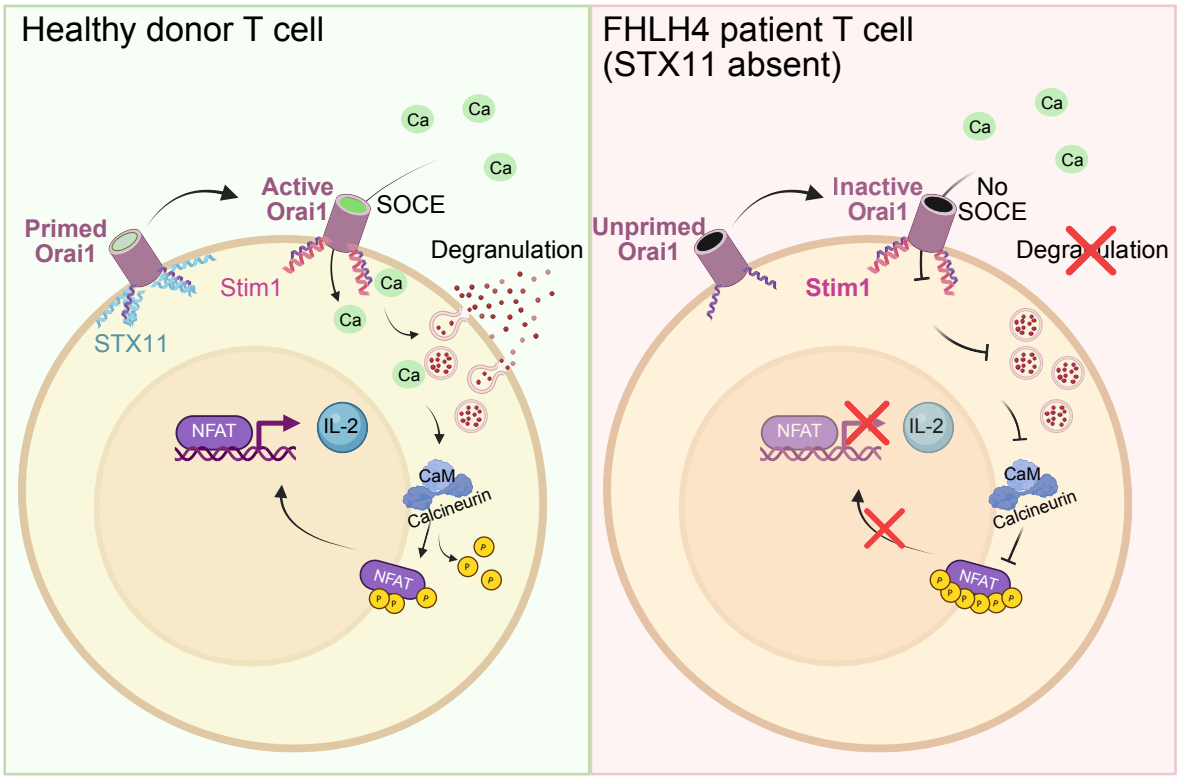

Supplementary Figure 1

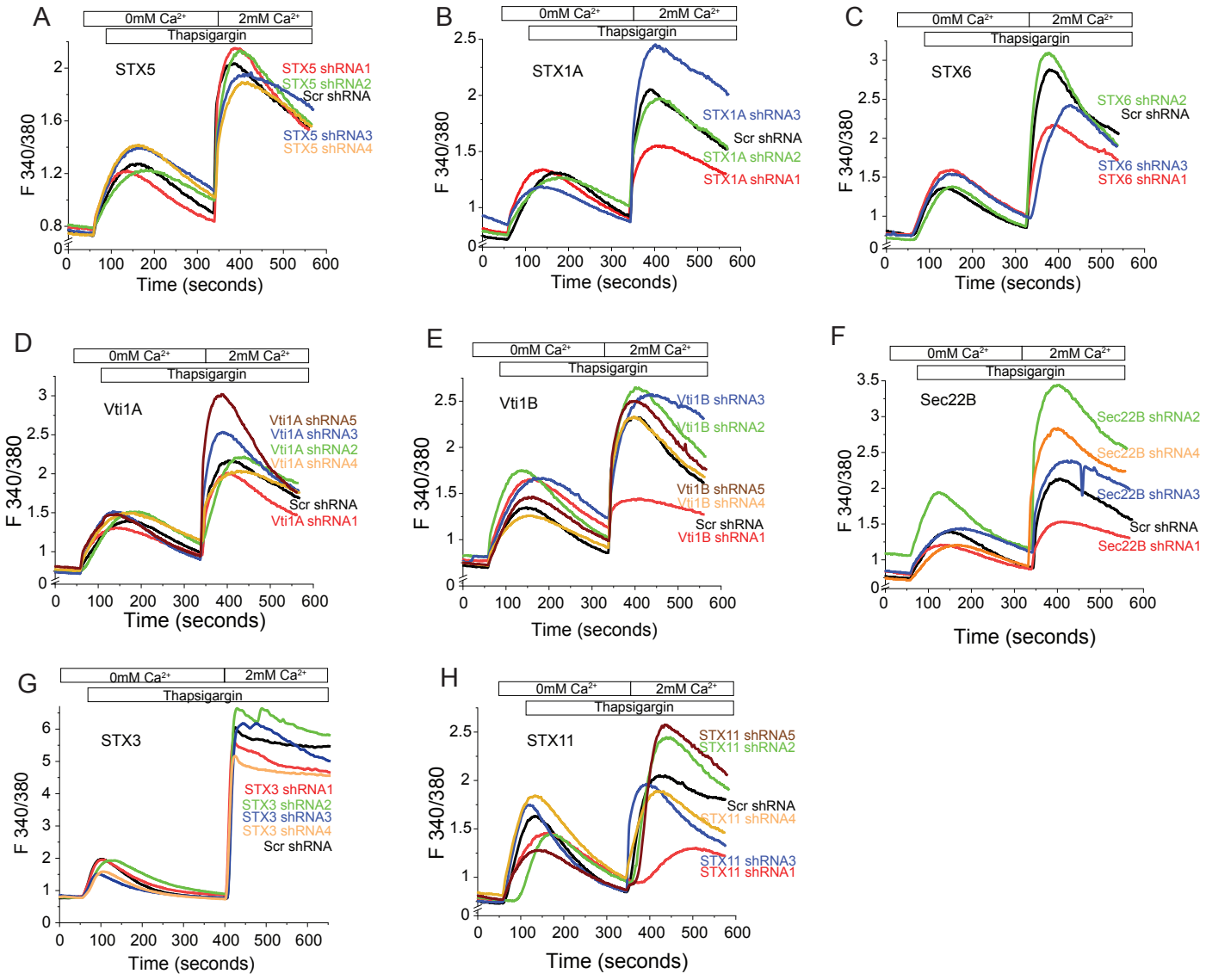

Supplementary Figure 1. (A-H) Targeted RNAi screen for SNAREs involved in SOCE. Fura-2 calcium imaging assays measuring thapsigargin (TG) induced SOCE in HEK293 and/or Jurkat cell lines treated with scramble (scr) shRNA or different shRNA sequences against the gene of interest for 3-4 days. Shown here are the average traces from 30-40 cells per group.

Supplementary Figure 2

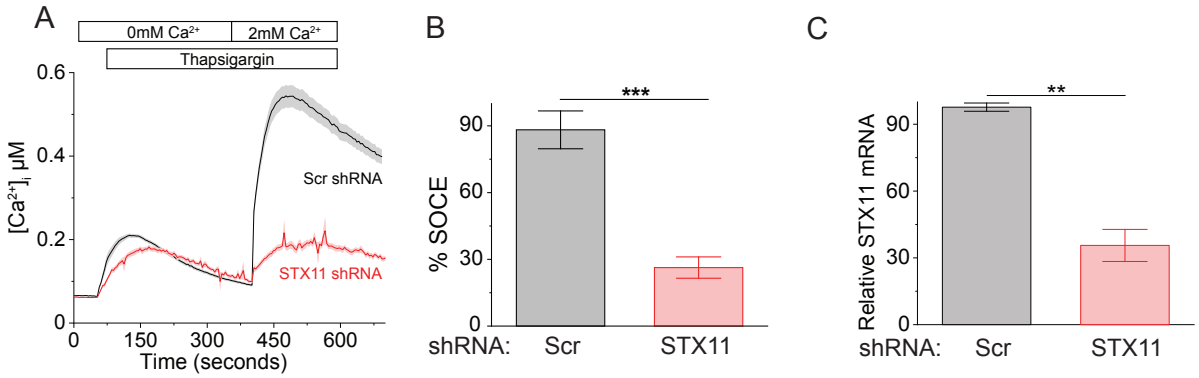

Supplementary figure 2 (A-B) Representative Fura-2 calcium imaging assay **(A)** and its quantification from repeats **(B)** measuring thapsigargin (TG) induced SOCE in HEK293 cells treated with scr or STX11 shRNA. Bars show relative SOCE ± SE from three independent experiments in **(A)** where SOCE from scramble shRNA treated group in one experiment was set at 100%. **(C)** Representative quantitative PCR to assess the efficiency of knockdown in shRNA treated cells from **(B)**. Total RNA extracted from cells treated with STX11 shRNA was subjected to qPCR analysis using Taqman probes for STX11. Data were normalized to Beta-actin housekeeping control.

Supplementary Figure 3

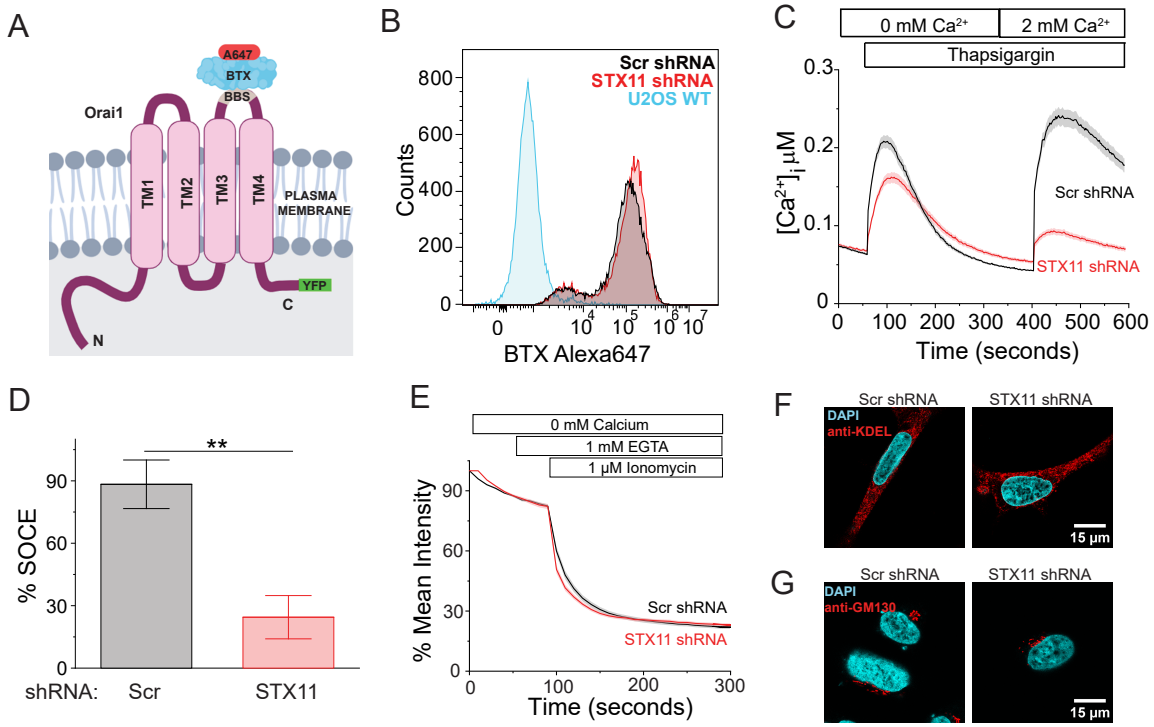

Supplementary Figure 3. (A) Schematic showing the design of recombinant Orai1-BBS-YFP fusion protein. Shown here is the placement of the bungarotoxin binding site (BBS) inside the second extracellular loop and YFP tag in the C-terminus of Orai1 as well as binding of BTX-A647 to BBS. **(B)** Quantification of total Orai1 levels in the plasma membrane of STX11 depleted cells. U2OS cells stably expressing Orai1-BBS-YFP were transduced with scr (black) or STX11 (red) shRNA, stimulated with 1uM TG, incubated with alpha-bungarotoxin alexa 647 (BTX-A647) and washed. BTX binding to surface Orai1 was measured using flow-cytometer, where its binding to wildtype U2OS cells were used as control. (N=3). **(C-D)** Measurement of thapsigargin (TG) induced SOCE in U2OS cells treated with STX11 RNAi in **(B)**. **(C)** Representative average single cell Fura-2 calcium imaging assay. **(D)** Bars showing relative mean % SOCE ± SE from three independent experiments in **(C)**. **(E)** Measurement of ER calcium content in Scr and STX11 shRNA treated HEK293 cells using ER-localized CEPIA. Cells were incubated in Ringer's buffer containing 0 mM calcium followed by 1 mM EGTA and stimulated with 1 uM ionomycin. (N=3).**(F-G)** Immunolabelling of HEK293 cells to assess ER **(F)** and Golgi **(G)** health. Scr and STX11 shRNA treated HEK293 cells were fixed, permeabilized and stained with anti-KDEL antibody **(F)** and anti-GM130 antibody **(G)** to assess ER and Golgi morphology respectively.

Supplementary Figure 4

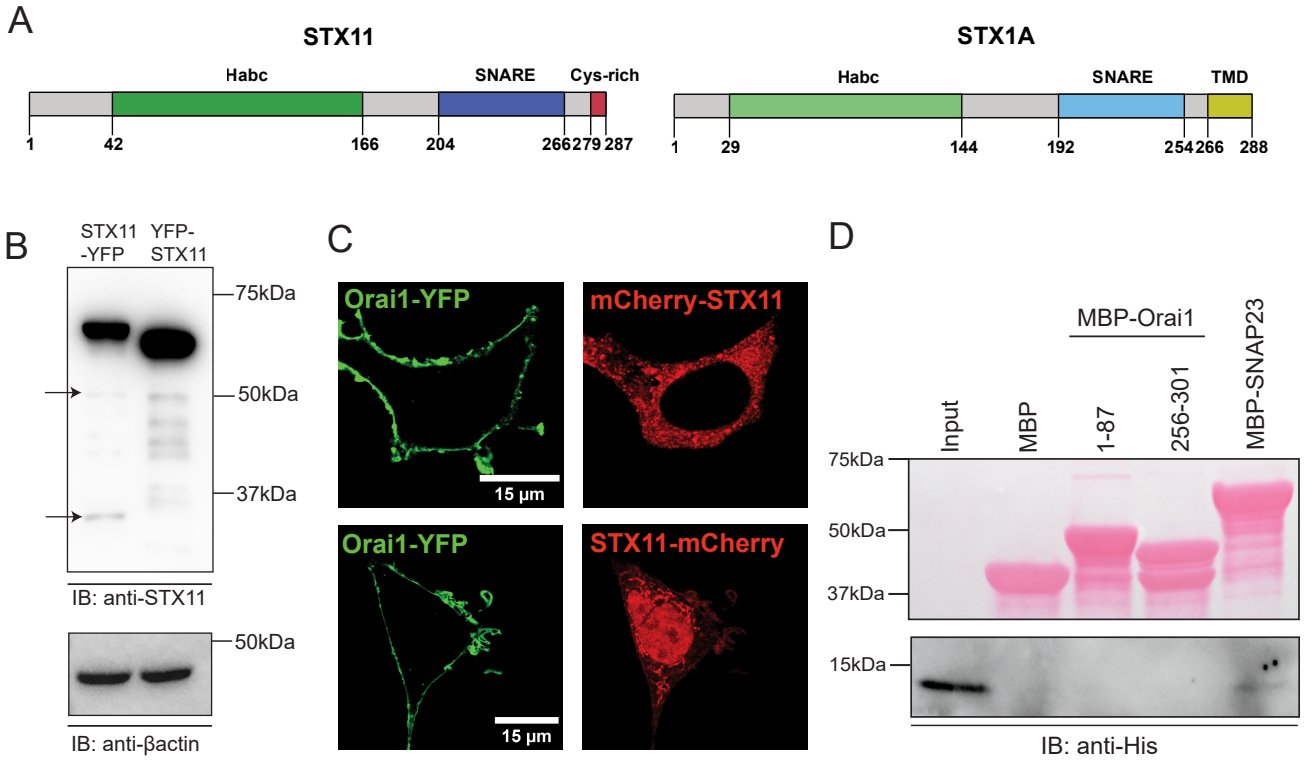

Supplementary Figure 4. (A) Schematic showing a comparison of the key domains in STX11 and STX1A. **(B)** Western blot of whole cell lysates prepared from HEK293 cells expressing YFP-STX11 and STX11-YFP. Note the mismatch in molecular weight of the N- versus C-terminally tagged STX11 and the degradation products (arrows). N=3. **(C)** Confocal images showing localization of ectopically expressed mCherry-STX11 or STX-11-mCherry in HEK293 cells. N=3. **(D)** Pull-down assay showing *in vitro* binding of His-tagged SNARE domain of STX11 to MBP-tagged Orai1 N- and C-termini. (Top panel) Ponceau S staining showing the input of MBP alone or MBP-tagged Orai1 cytosolic tails. (Bottom panel) Western blot using anti-His antibody.

Supplementary Figure 5

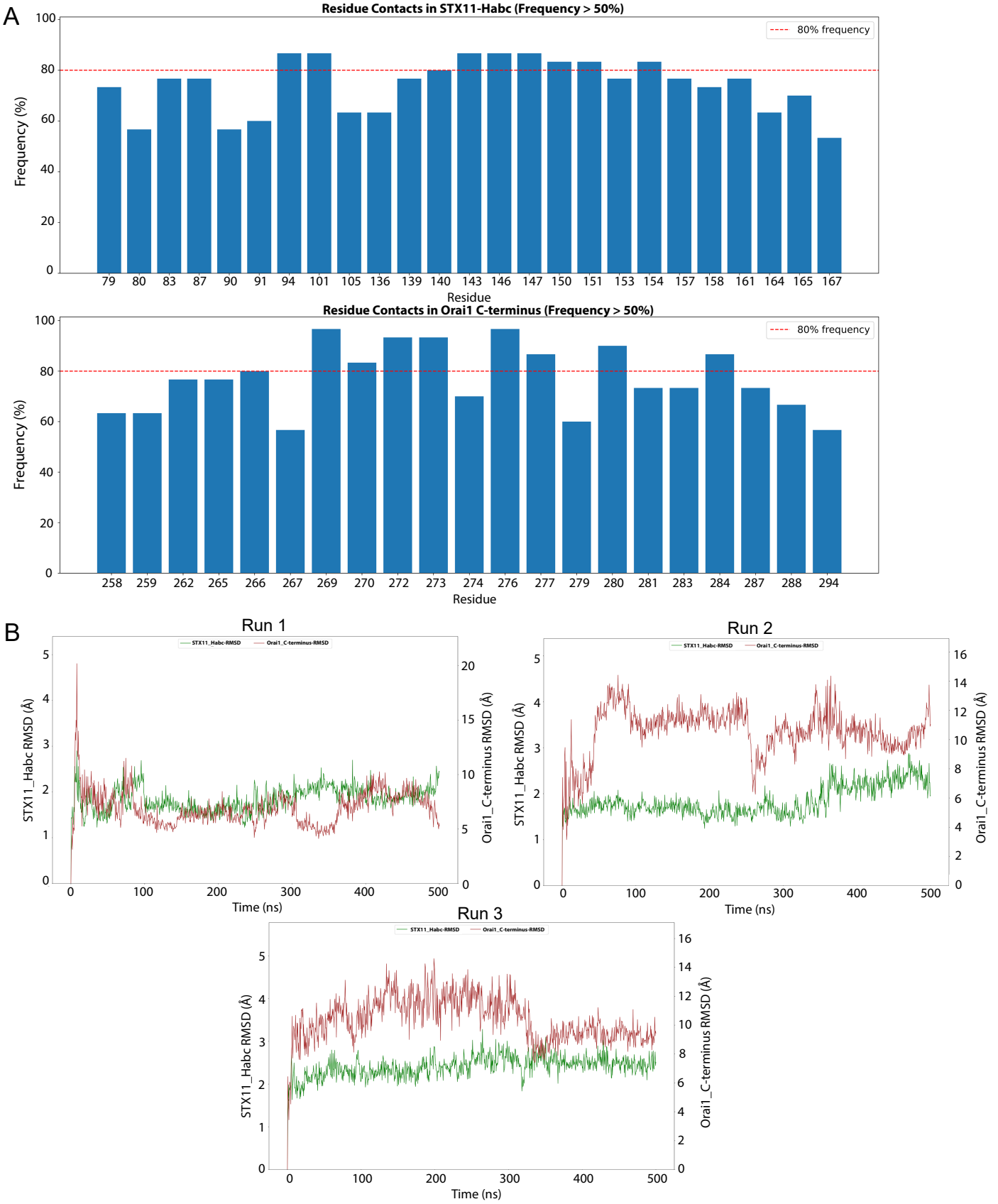

Supplementary Figure 5: (A) Frequency of interface residues of STX11-H_{abc} and Orai1 C-terminus across AF3 predicted models. Residues with more than 50% frequency are shown. **(B)** RMSD of STX11 H_{abc} and Orai1 C-terminus upon superposition on the 0th ns frame. The STX11-H_{abc} RMSD indicates the backbone RMSD upon superposition of all frames on the STX11-H_{abc} backbone of 0th ns. The Orai1 C-terminus RMSD suggests the stability of Orai1 with respect to STX11 and is calculated for the Orai1 C-terminus after superposition of all frames on the STX11-H_{abc} backbone of 0th ns.

Supplementary Figure 6

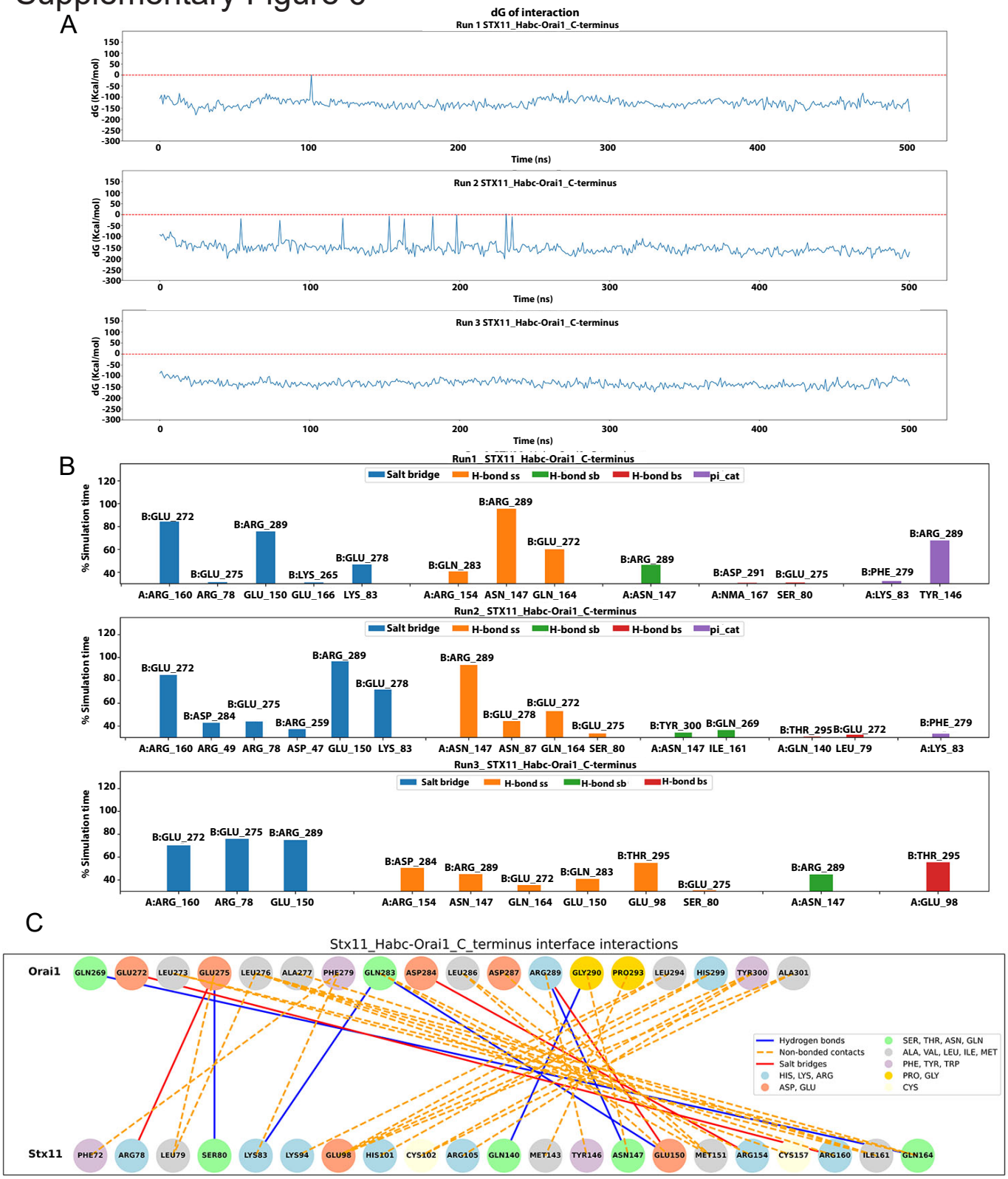

Supplementary Figure 6: (A) Binding energy (ΔG) of STX11-H_{abc} and Orai1 C-terminus complex across the simulation time for all three replicates. **(B)** Interactions between STX11-H_{abc} and Orai1 C-terminus across the simulation time in three replicates. The interactions that persist for more than 30% of simulation time are shown and highlighted in different colors. H-bond has been categorized as sidechain-sidechain (ss), sidechain-backbone (sb) and backbone-sidechain (bs). **(C)** Residues predicted to be involved in interaction between STX11 H_{abc} and the Orai1 C-terminus identified from all-atom MD simulations.

Supplementary Figure 7

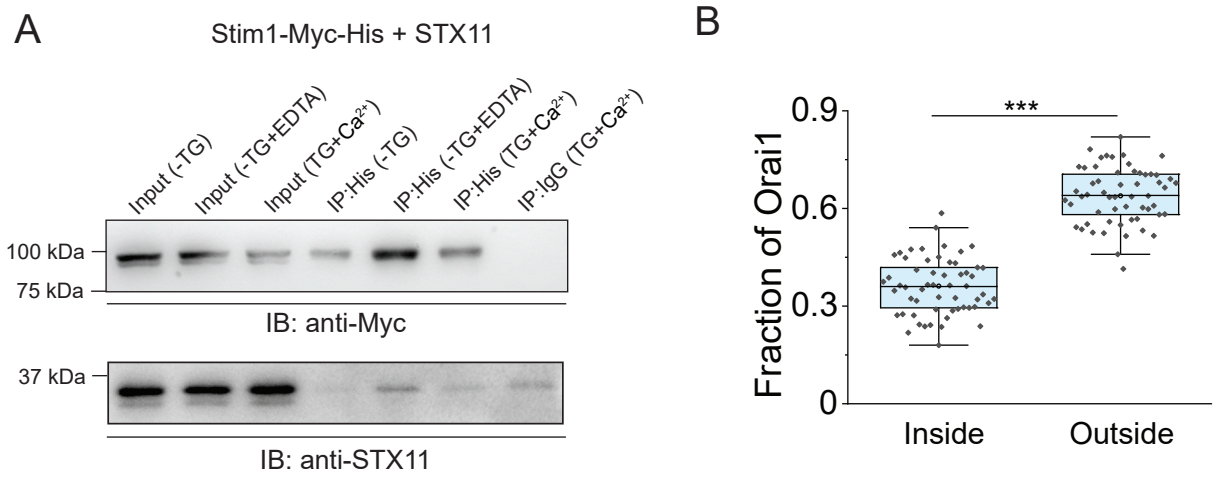

Supplementary Figure 7. (A) Co-immunoprecipitation (co-IP) to test the association of Stim1 with STX11. HEK293 cells were co-transfected with Stim1-Myc-His and STX11, store-depleted, lysed and subjected to co-IP followed by Western blot as indicated. (N=2) **(B)** Quantification of fraction of Orai1 inside and outside Stim1:Orai1 clusters in store-depleted HEK293 cells expressing CFP-Orai1 and Stim1-YFP.

Supplementary Figure 8

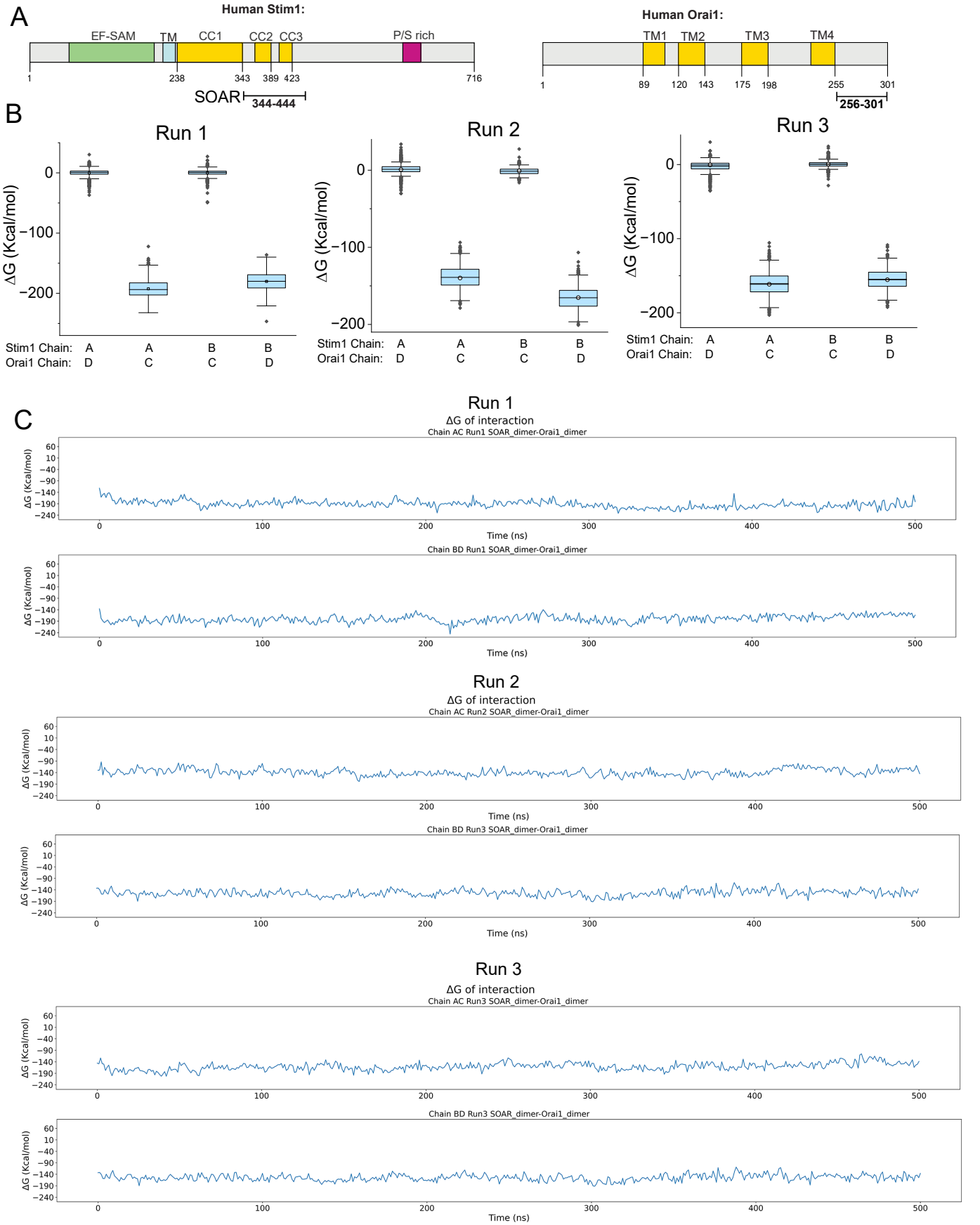

Supplementary Figure 8: (A) Schematic of human Stim1 and Orai1 showing the domains used for MD simulation. TM:Transmembrane, P/S: Proline/Serine rich and CC: represent Coiled coil domains. **(B)** The binding free energy distribution of the three runs for the interactions between the SOAR dimer and Orai1 C termini. **(C)** Binding energy (Δ G) of SOAR dimer and Orai1 C-termini complex across the simulation time for all three runs.

Supplementary Figure 9

A

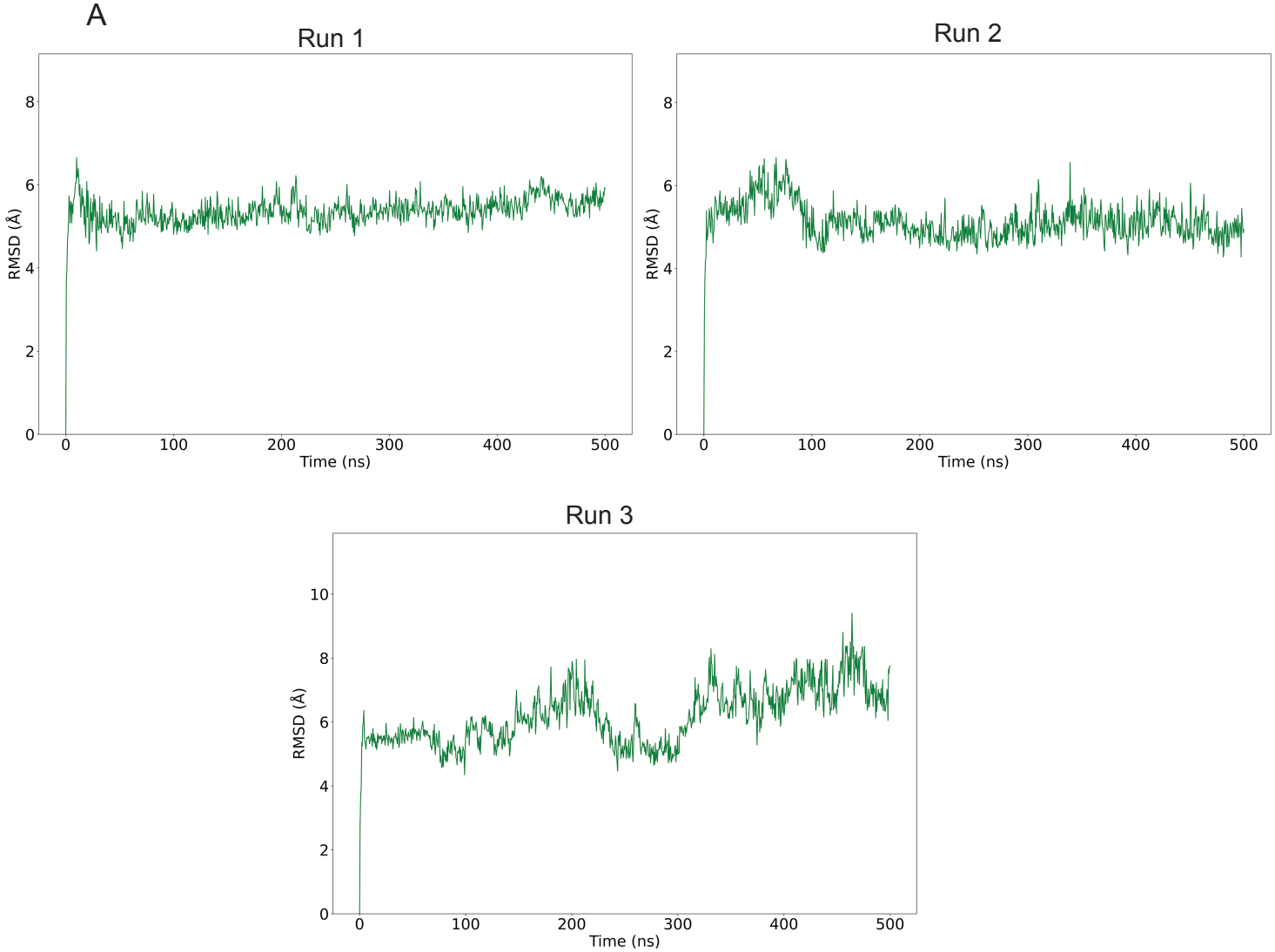

B

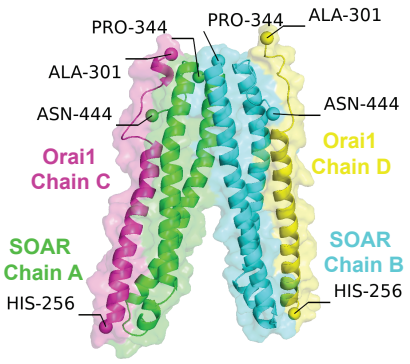

Supplementary Figure 9. (A) RMSD of SOAR dimer and Orai1 C-termini. **(B)** Cartoon representation of the structure of Stim1-SOAR(344-444) dimer in complex with Orai1 C-termini.

Supplementary Figure 10

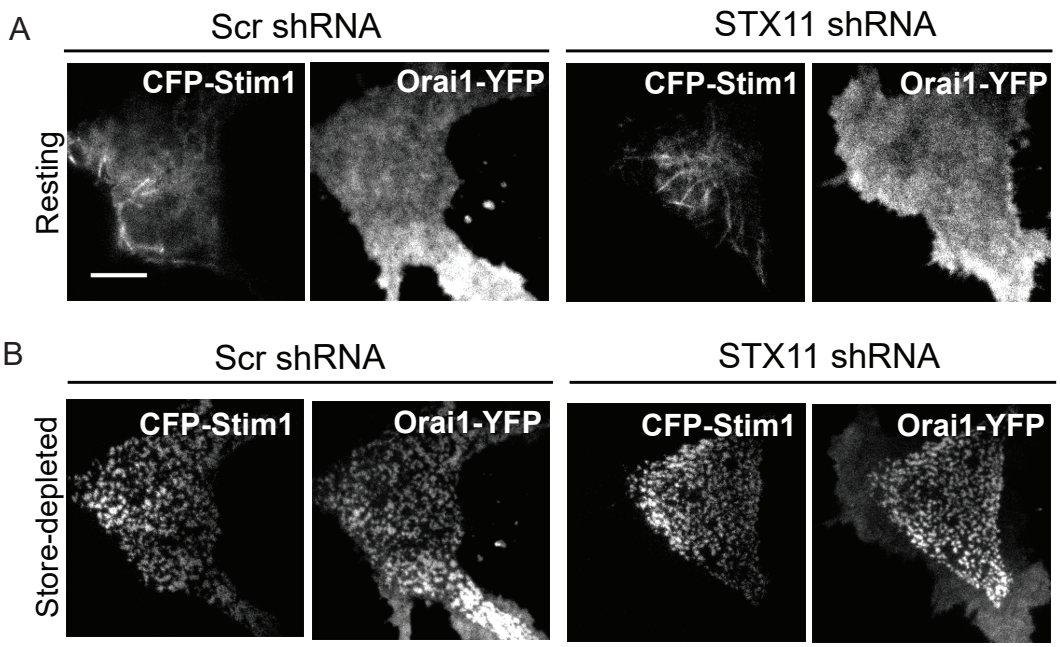

Supplementary Figure 10. (A-B) Orai1-YFP and CFP-Stim1 clusters in control and STX11 depleted cells. Representative images of Scr and STX11 shRNA treated resting **(A)** and store-depleted **(B)** HEK293 cells expressing C-terminal YFP-tagged Orai1 (Orai1-YFP) and N-terminal CFP-tagged Stim1 (CFP-Stim1). Scale bar 10μm.

Supplementary Figure 11

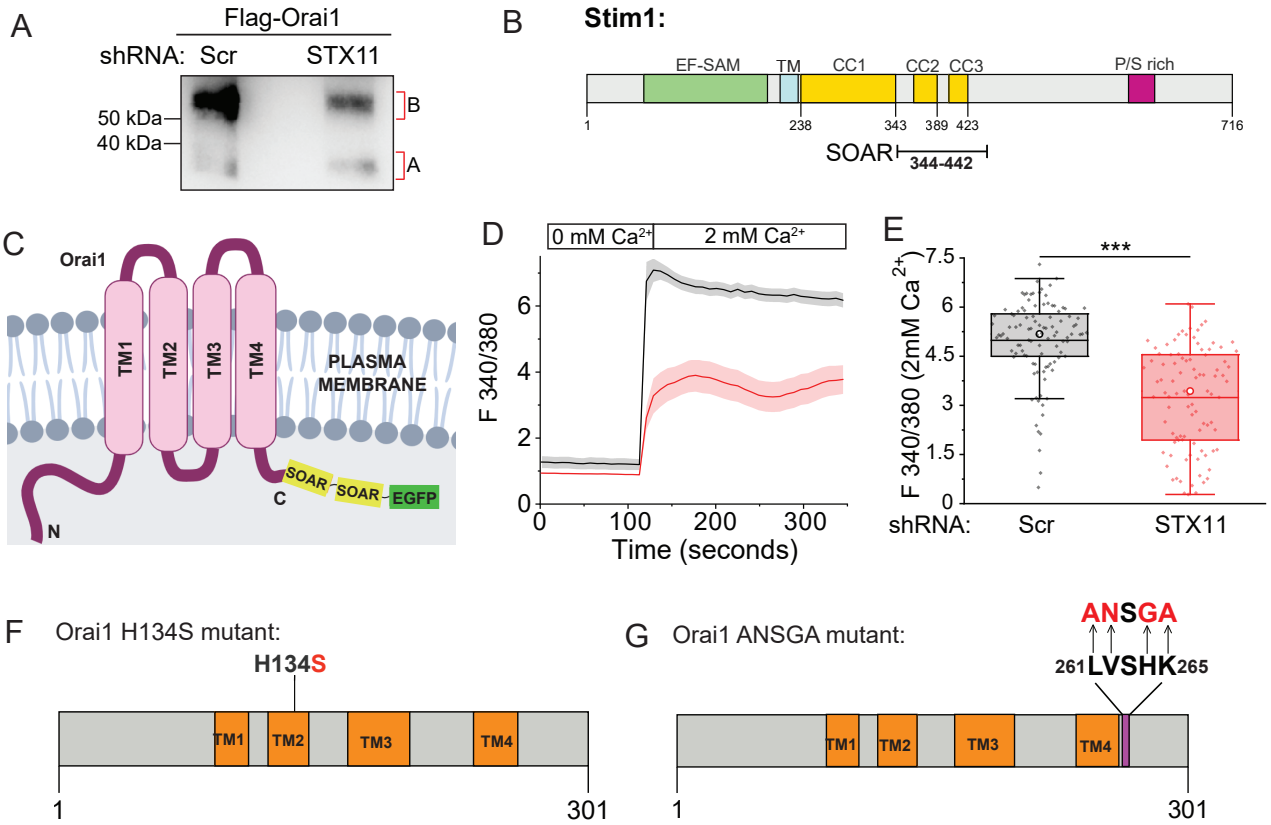

Supplementary Figure 11. (A) Western blot of BS3 cross-linked Flag-Orai1 acquired at a higher exposure showing the monomeric Flag-Orai1 band (labelled as A) **(B)** Schematic representation of SOAR domain in full length Stim1. **(C)** Cartoon showing the design of the Orai1-SOAR-SOAR-EGFP (Orai1-S-S-GFP) construct. **(D)** Representative Fura-2 calcium imaging assay to measure constitutive calcium influx in Orai1-S-S-GFP expressing control (black) or STX11 depleted (red) HEK293 cells. Cells were imaged in Ringer's buffer containing 0 mM followed by 2 mM extracellular Ca^{2+}. **(E)** Quantification of constitutive calcium influx across experiments as shown in **(D)**. N=3. **(F-G)** Schematic representations of H134S mutation **(F)** and ANSGA mutation **(G)** in full length Orai1.

Supplementary Figure 12

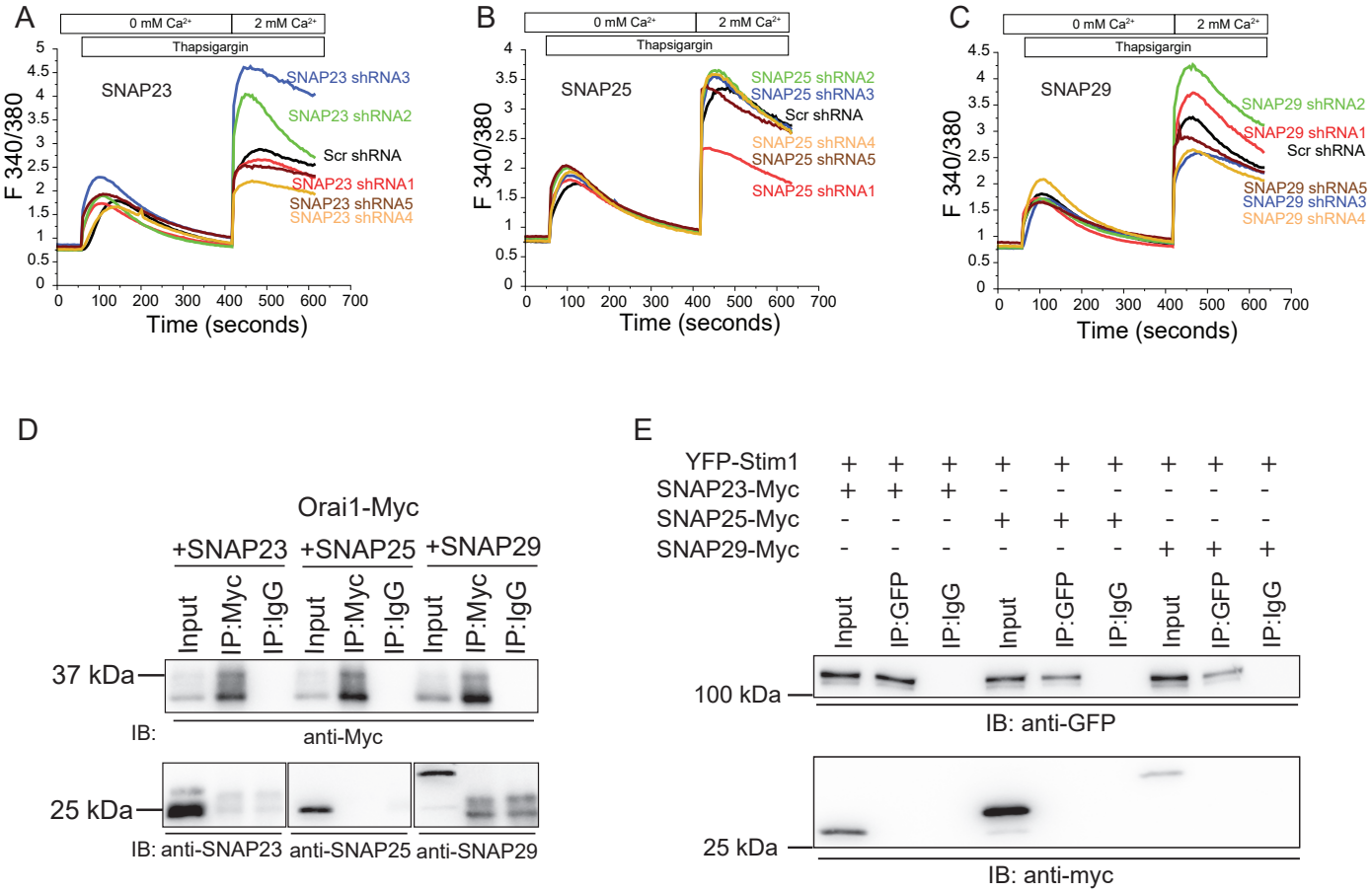

Supplementary Figure 12. SOCE in RNAi treated Jurkat cells to assess the role of SNAPs. **(A-C)** Fura-2 calcium imaging assay measuring SOCE in cells treated with scramble (scr) shRNA or different shRNA sequences against SNAP23 **(A)** SNAP25 **(B)** SNAP29 **(C)**. Average traces from 30-40 cells per group are shown. **(D)** Western blot images of co-IPs to test the association of Orai1 with SNAP23/ SNAP25/ SNAP29. HEK293 cells were co-transfected with Orai1-Myc and untagged SNAP23/ SNAP25/ SNAP29, store-depleted, lysed and subjected to co-IP followed by western blot as indicated. (N=2) **(E)** Western blot images of co-IP to test the association of Stim1 with SNAP23/ SNAP25/ SNAP29. HEK293 cells were co-transfected with YFP-Stim1 and Myc-tagged SNAP23/ SNAP25/ SNAP29, store-depleted, lysed and subjected to co-IP followed by western blot as indicated. (N=2).

Supplementary figure 13

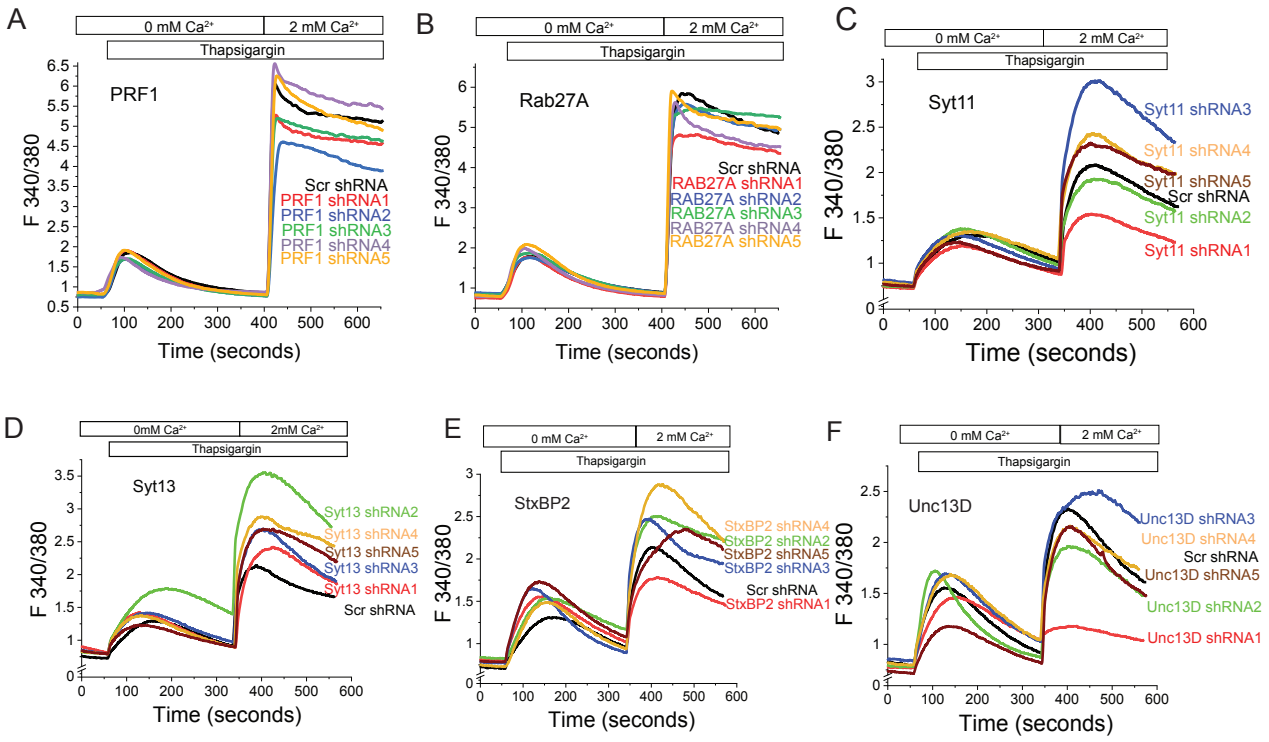

Supplementary Figure 13. RNAi screen for genes involved in primary HLH and/or vesicle fusion for their role in SOCE. **(A-F)** Fura-2 calcium imaging assays measuring thapsigargin (TG) induced SOCE in HEK293 or Jurkat cells treated with scramble (scr) shRNA or different shRNA sequences against the gene of interest for 3-4 days. Shown here are the average traces from 30-40 cells per group.

Supplementary Table 1: AF3 prediction for STX11:Orai1 complex formation

Proteins/Domains	ipTM	pTM
Full-length Orai1 - Full-length STX11	0.11	0.35
STX11-Habc_41-167 and Orai1_N-term_1-87	0.27	0.59
STX11-Habc_41-167 and Orai1_C-term_256-301	**0.53**	**0.79**
STX11-SNARE_183-267 and Orai1_N-term_1-87	0.08	0.34
STX11-SNARE_183-267 and Orai1_C-term_256-301	0.18	0.45
STX11-Habc_41-167 and full-length Orai1	0.24	0.38
STX11-SNARE_183-267 and full-length Orai1	0.08	0.37
Orai1_N-term_1-87 and full-length STX11	0.15	0.5
Orai1_C-term_256-301 and full-length STX11	0.16	0.54

Supplementary Table 2: AF3 predictions for STX11-H_{abc} and Orai1 C-terminus with different seeds

Seed values for STX11-H_{abc} and Orai1 C-terminus	ipTM	pTM
111	**0.69**	**0.85**
236	0.51	0.78
174	0.5	0.77
802	0.49	0.76
455	0.56	0.78

Supplementary Table 3: AF3 predictions for SOAR and Orai1 in 2:2 ratio

2 copies of SOAR and 2 copies of Orai1_C-term_256-301	ipTM	pTM
Seed_101	0.73	0.78
Seed_102	0.73	0.78
Seed_103	0.73	0.78
Seed_104	0.73	0.78
Seed_105	**0.74**	**0.79**